Human chromokinesins promote chromosome congression and spindle microtubule dynamics during mitosis

Cornelia Wandke,[1,2] Marin Barisic,[1,3] Reinhard Sigl,[1] Veronika Rauch,[1] Frank Wolf,[1] Ana C. Amaro,[2] Chia H. Tan,[2] Antonio J. Pereira,[3] Ulrike Kutay,[2] Helder Maiato,[3,4] Patrick Meraldi,[2] and Stephan Geley[1]

[1]Biocenter, Division of Molecular Pathophysiology, Innsbruck Medical University, A-6020 Innsbruck, Austria
[2]Institute of Biochemistry, ETH, 8093 Zurich, Switzerland
[3]Chromosome Instability and Dynamics Laboratory, Institute for Molecular and Cellular Biology, and [4]Department of Experimental Biology, Faculdade de Medicina, Universidade do Porto, 4099-002 Porto, Portugal

Chromokinesins are microtubule plus end–directed motor proteins that bind to chromosome arms. In *Xenopus* egg cell-free extracts, Xkid and Xklp1 are essential for bipolar spindle formation but the functions of the human homologues, hKID (KIF22) and KIF4A, are poorly understood. By using RNAi-mediated protein knockdown in human cells, we find that only co-depletion delayed progression through mitosis in a Mad2-dependent manner. Depletion of hKID caused abnormal chromosome arm orientation, delayed chromosome congression, and sensitized cells to nocodazole. Knockdown of KIF4A increased the number and length of microtubules, altered kinetochore oscillations, and decreased kinetochore microtubule flux. These changes were associated with failures in establishing a tight metaphase plate and an increase in anaphase lagging chromosomes. Co-depletion of both chromokinesins aggravated chromosome attachment failures, which led to mitotic arrest. Thus, hKID and KIF4A contribute independently to the rapid and correct attachment of chromosomes by controlling the positioning of chromosome arms and the dynamics of microtubules, respectively.

Introduction

The faithful segregation of chromosomes during mitosis requires a tight temporo-spatial coordination between nuclear and cellular division. These events are timed by ordered proteolysis that controls the onset of anaphase and exit from mitosis (Nasmyth, 2002). In addition, chromosomes must also be spatially organized such that the cleavage furrow can intersect precisely between the two sets of separating sister chromatids during anaphase and telophase. Hence, it is important to understand how chromosomes congress to the metaphase plate and whether and how achieving this spatial arrangement contributes to the accurate segregation between the two daughter cells to avoid aneuploidy, which is considered tumorigenic (Gordon et al., 2012).

Chromosome alignment at the metaphase plate, a conserved feature of mitosis in eukaryotes, is influenced by many different factors, including regulation of kinetochore microtubule (MT) dynamics, e.g., by kinesin-8 motors (Garcia et al., 2002;

West et al., 2002; Gupta, Jr. et al., 2006; Varga et al., 2006; Mayr et al., 2007; Stumpff et al., 2008, 2011; Du et al., 2010; Wargacki et al., 2010), plus end–directed transport of chromosomes along MTs by CENP-E (Kapoor et al., 2006; Kim et al., 2010), and polar ejections forces (PEFs; Rieder et al., 1986; Cassimeris et al., 1994; Rieder and Salmon, 1994; Antonio et al., 2000; Funabiki and Murray, 2000; Levesque and Compton, 2001; Marshall et al., 2001; Brouhard and Hunt, 2005; Ke et al., 2009; Bieling et al., 2010a; Stumpff et al., 2012). In contrast to the first two mechanisms, which directly impinge on chromosome movements by acting on kinetochores, how PEFs could contribute to chromosome congression remains unclear.

Chromokinesins are abundant chromosome-bound MT motor proteins (Yajima et al., 2003; Bringmann et al., 2004; Bieling et al., 2010a; Stumpff et al., 2012) harboring an N-terminal motor and a C-terminal chromatin interaction domain

The Rockefeller University Press $30.00
J. Cell Biol. Vol. 198 No. 5   847–863
www.jcb.org/cgi/doi/10.1083/jcb.201110060

JCB   **847**

Figure 1. **Chromokinesin knockdown results in prometaphase arrest.** (A) Total cell extracts prepared from HeLa cells 36 h post-transfection (pt) with siRNAs were analyzed by immunoblotting for KIF4A, hKID, and α-tubulin. (B) HeLa cells transfected with 50 nM of siRNAs targeting hKID, KIF4A, or both (KK) were methanol-fixed 40 h pt, DNA stained, and the mitotic index and (C) the mitotic phases determined (mean of three independent experiments + SEM).

(Mazumdar and Misteli, 2005). These MT plus end–directed motors were proposed to contribute to chromosome anti-poleward (AP) movements and formation of the metaphase plate (Rieder et al., 1986; Cassimeris et al., 1994; Rieder and Salmon, 1994; Antonio et al., 2000; Funabiki and Murray, 2000; Levesque and Compton, 2001; Brouhard and Hunt, 2005; Ke et al., 2009; Bieling et al., 2010a; Stumpff et al., 2012).

One of the two human chromokinesins, hKID (KIF22), has been shown to contribute strongly to AP movements and the PEF (Levesque and Compton, 2001; Brouhard and Hunt, 2005; Santamaria et al., 2008; Cochran et al., 2009; Barisic et al., 2010). hKID, a member of the kinesin 10 family (Yajima et al., 2003), is closely related to *Drosophila* Nod, a nonprocessive motor that binds to MT plus-ends and drives chromosome movements. The *Xenopus laevis* homologue Xkid (54% identity) is essential for the proper alignment of chromosomes of in vitro–assembled bipolar spindles (Antonio et al., 2000; Funabiki and Murray, 2000), whereas RNAi-based studies in human cells or gene-targeted mice revealed only minor problems in chromosome congression and alignment at the metaphase plate (Levesque and Compton, 2001; Levesque et al., 2003; Tokai-Nishizumi et al., 2005; Zhu et al., 2005; Ohsugi et al., 2008). hKID was, however, found to set spindle length (Tokai-Nishizumi et al., 2005) and to control chromosome arm orientation and oscillation (Levesque and Compton, 2001; Magidson et al., 2011). Interestingly, hKID was required for chromosome alignment in cells in which the spindle pole–organizing protein NUMA was inhibited (Levesque et al., 2003). Thus, although the functions of hKID as a motor able to push chromosome arms and exert forces on the bipolar spindle (Oshimori et al., 2006; Logarinho et al., 2012) are well established, the significance of these functions for mitosis in somatic cells is still unclear.

The other chromokinesin, KIF4, a member of the kinesin 4 family, contributes to various aspects of mitosis. In *Caenorhabditis elegans,* KLP-19 is required for metaphase plate formation. In contrast to other KIF4 homologues, KLP-19 generates PEF and is, therefore, functionally more similar to hKID (Powers et al., 2004). In *Drosophila*, Klp3A controls mitotic spindle length (Kwon et al., 2004) and is essential for cytokinesis (Williams et al., 1995). The *Xenopus* homologue Xklp1 was found to be required for chromosome congression (Vernos et al., 1995), to regulate MT dynamics in vitro, and to control MT density of spindles (Bringmann et al., 2004; Castoldi and Vernos, 2006). RNAi-based analysis in human cells showed that KIF4A is involved in chromosome congression and cytokinesis (Kurasawa et al., 2004; Mazumdar et al., 2004; Zhu and Jiang, 2005; Zhu et al., 2005). KIF4A can also control MT dynamics, at least during anaphase and telophase, which is important for proper spindle midzone formation (Kurasawa et al., 2004; Zhu and Jiang, 2005; Hu et al., 2011). Recent work suggests that KIF4A also directly suppresses MT growth during earlier stages of mitosis (Stumpff et al., 2012). In addition to its impact on MT dynamics, KIF4A has been shown to interact with condensin complexes, which could alter the elastic properties of chromosomes and, therefore, affect chromosome congression (Jaqaman et al., 2010). The mechanism and timing of KIF4 control on MT dynamics as well as its effect on chromosome condensation during mitosis are, however, only poorly understood, and it is not well established how these parameters contribute to the chromosome congression defects observed in previous RNAi studies (Mazumdar et al., 2004; Zhu et al., 2005).

Thus, although the biochemical analysis of Xklp1 and Xkid demonstrated essential functions for bipolar spindle formation, chromosome congression, and segregation in *Xenopus* egg extract–based in vitro experiments, RNAi-based experiments in human cells revealed only minor chromosome congression defects after depletion of either KIF4A or hKID. Because chromosome congression in human cells is largely controlled by the dynamics of kinetochore MTs, a major open question is whether and how chromokinesins can exert their effect via regulation of MT dynamics. Here, we have assessed the potential redundancy of human chromokinesins in knockdown and knockout experiments and found that chromokinesins promote efficient chromosome congression through the concerted generation of AP force and the regulation of spindle MT dynamics.

Results

Chromokinesin knockdown results in checkpoint-dependent prometaphase arrest

To determine the role of chromokinesins in spindle formation during mitosis, we performed RNAi knockdown experiments of either hKID, KIF4A, or both (KK) in human HeLa cells. Transient siRNA transfection resulted in a reduction of at least 95% of the respective protein levels as determined by immunoblotting (Fig. 1 A). Most of the following experiments were performed with two independent siRNA sequences with similar outcome. Knockdown of hKID caused shortened mitotic spindles from 8.70 ± 0.68 μm in controls ($n = 52$) to 7.77 ± 0.64 μm ($n = 51$) in hKID-depleted cells (Fig. 1 D) and slightly increased the mitotic index from $6.1 \pm 0.1\%$ in control to $7.3 \pm 0.3\%$ in hKID RNAi cells (Fig.1, B and C; Table 1). When progression through mitosis was monitored in HeLa cells expressing histone H2B-GFP, the duration of early mitosis, i.e., the time from the onset of chromosome condensation to anaphase onset, was increased from 35 min (median, $n = 275$) in control to 40 min ($n = 506$) in hKID-depleted cells (Fig. S1, A and B; Table 1). This delay in mitosis was associated with a higher frequency of noncongressed chromosomes (8.8% in controls to 19.7% upon hKID depletion), suggesting that hKID is involved in chromosome

(D) Maximum intensity projections (MIP) of deconvolved z-stacks showing representative mitotic spindles of different siRNA treatments. Arrows indicate the misoriented chromosome arms and uncongressed chromosomes in hKID/KIF4A RNAi. Arrowheads mark stabilized, aberrant nonkinetochore MTs in KIF4A knockdown cells. Note the increased interkinetochore distance (sister separation) in KIF4A and KK knockdown cells (arrowhead with asterisk). Bar, 5 μm. (E) Quantification of chromosome congression failures from mitotic cells of three independent experiments. (F) HeLa cells were transfected with different siRNAs and treated with 15 nM nocodazole or solvent 24 h later. After 12 h treatment, cells were imaged and analyzed for their mitotic index. Mean ± SEM of three independent experiments. Student's *t* test significance values: *, $P < 0.05$; **, $P < 0.01$; ***, $P < 0.001$.

Table 1. **Summary of the effects of hKID, KIF4A, and hKID/KIF4A RNAi in human cells**

Parameter\Treatment	Control RNAi	hKID RNAi	KIF4A RNAi	hKID/KIF4A RNAi
Mitotic index (MI) (mean ± SEM)	6.1 ± 0.1%	7.3 ± 0.3% (*)	6.7 ± 0.3%	17.9 ± 1.2% (*)
Length of mitosis (median; Q1; Q3)	35; 30; 40 min	40; 35; 60 min	40; 30; 60 min	90; 65; 150 min (***)
Prometaphases (mean ± SEM)	30.7 ± 3.2%	42.5 ± 1.6% (*)	38.4 ± 5.7%	78.4 ± 3.9% (***)
Lagging chromosomes (mean ± SEM)	3.19 ± 0.52%	10.77 ± 3.4%	11.69 ± 2.05%	25.7 ± 2.25% (*)
Cytokinesis failures (mean ± SEM)	2.37 ± 1.1%	1.1 ± 0.4%	4.85 ± 1.8%	10.45 ± 0.41%
≥3 uncongressed chromosomes	8.8%	19.7%	18.0%	62.5%
Cell death (mean ± SD)	1.85 ± 0.31%	2.23 ± 0.26%	3.06 ± 0.25% (*)	4.09 ± 0.75%
Bipolar spindle size (mean ± SD)	8.70 ± 0.68 µm	7.77 ± 0.64 µm (***)	8.53 ± 0.73 µm	9.94 ± 1.36 µm (***)
Monopolar spindles (mean ± SEM)	3.98 ± 0.08 µm	3.12 ± 0.11 µm (***)	3.78 ± 0.06 µm	2.85 ± 0.06 µm (***)
IK distance (mean ± SD)	1.01 ± 0.08 µm	1.00 ± 0.07 µm	1.27 ± 0.09 µm (***)	1.24 ± 0.10 µm (***)
Oscillation half period (τx)	52.5 s	52.5 s	60 s	75 s
Oscillation speed (mean ± SD)	1.23 ± 0.21 µm/min	1.13 ± 0.18 µm/min (**)	1.13 ± 0.21 µm/min (*)	1.12 ± 0.17 µm/min (**)
Nocodazole sens. MI (mean ± SEM)	9.9 ± 0.8% (*)	22.7 ± 1.1% (**)	4.5 ± 0.3%	31.9 ± 1.4% (**)
MT density (EB1-GFP)(mean ± SEM)	17.7 ± 0.01	14.6 ± 0.03	23.5 ± 0.01 (*)	ND
MT life time (EB3-YFP) (mean ± SD)	3.7 ± 0.5 s	3.5 ± 0.4 s	5.6 ± 0.6 s (***)	5.8 ± 0.7 s (***)
MT flux (mean ± SEM)	0.62 ± 0.12 µm/min	0.55 ± 0.11 µm/min	0.34 ± 0.13 µm/min (***)	0.47 ± 0.10 µm/min (***)

Experiments were performed in HeLa cells except for MT flux and turnover measurements, which were done in U2OS cells. ND, not determined; IK, interkinetochore; sens., sensitivity. *, **, and *** represent Student's t test P-values of <0.05, <0.01, and <0.001, respectively.

congression (Fig. 1, C and E; Table 1), confirming earlier studies (Theurkauf and Hawley, 1992; Antonio et al., 2000; Funabiki and Murray, 2000; Levesque and Compton, 2001; Goshima and Vale, 2003; Zhu et al., 2005). As reported previously, loss of hKID function also prevented the formation of the prometaphase chromosome ring and caused a higher number of anaphase-lagging chromosomes (Magidson et al., 2011).

In addition to chromosome arm–bound motors, like hKID, the pushing force of growing MTs interacting with chromosome arms could also contribute to the PEF and chromosome congression, as suggested by chromosome arm–shortening experiments (Ke et al., 2009). To investigate whether interfering with MT polymerization might enhance the hKID RNAi phenotype, we treated control and hKID RNAi cells with low doses of nocodazole (15 nM; Jordan et al., 1992). At this dose the mitotic spindle was not disrupted and only a slight prolongation of mitosis was observed in control RNAi cells. In hKID-depleted cells, however, the mitotic index rose from 7.3% in the solvent control to 22.7% upon nocodazole treatment, due to severe chromosome congression defects (Fig. 1 F; P < 0.01). These data support the hypothesis that MT dynamics or the density of MTs along chromosome arms might be important for efficient chromosome congression.

Because KIF4A is an abundant chromokinesin that could control the numbers and dynamics of MTs along chromosome arms, we investigated the role of KIF4A in chromosome alignment.

First, the KIF4A knockdown phenotype was determined in human cells. Knockdown of KIF4A prolonged mitosis slightly (Fig. 1 B; Fig. S1, A and B; median = 40 min, $n = 540$), and caused an increase in noncongressed chromosomes (Fig. 1 E) and a higher frequency of lagging chromosomes in anaphase (Fig. S1 C; Table 1). Mitotic spindles of KIF4A RNAi cells were of normal length (8.53 ± 0.73 µm; $n = 52$) but their morphology was slightly changed into a more barrel-like appearance, similar to in vitro spindles depleted of Xklp1 (Fig. 1 D; Castoldi and Vernos, 2006). In addition, KIF4A-depleted spindles were characterized by an increase in aberrant MTs (Fig. 1 D, small arrowheads) and exhibited a broader metaphase plate (Fig. 1 D, arrowheads with asterisk). As reported previously (Zhu and Jiang, 2005; Midorikawa et al., 2006; Hu et al., 2011), KIF4A knockdown prevented the formation of a spindle midzone and led to cytokinesis failure in 4.85% of transfected cells ($n = 540$, as compared with 2.37% in control RNAi cells [$n = 275$]; Fig. S1 C, Table 1). In summary, in agreement with earlier studies (Kurasawa et al., 2004; Tokai-Nishizumi et al., 2005; Zhu and Jiang, 2005; Mazumdar et al., 2006; Ohsugi et al., 2008), siRNA-mediated knockdown of hKID or KIF4A caused a higher frequency of misaligned chromosomes, but the majority of chromosomes managed to congress properly to the metaphase plate.

In contrast to the mild effects seen in the knockdown of the individual chromokinesins, knockdown of both proteins simultaneously resulted in a significantly lengthened mitosis
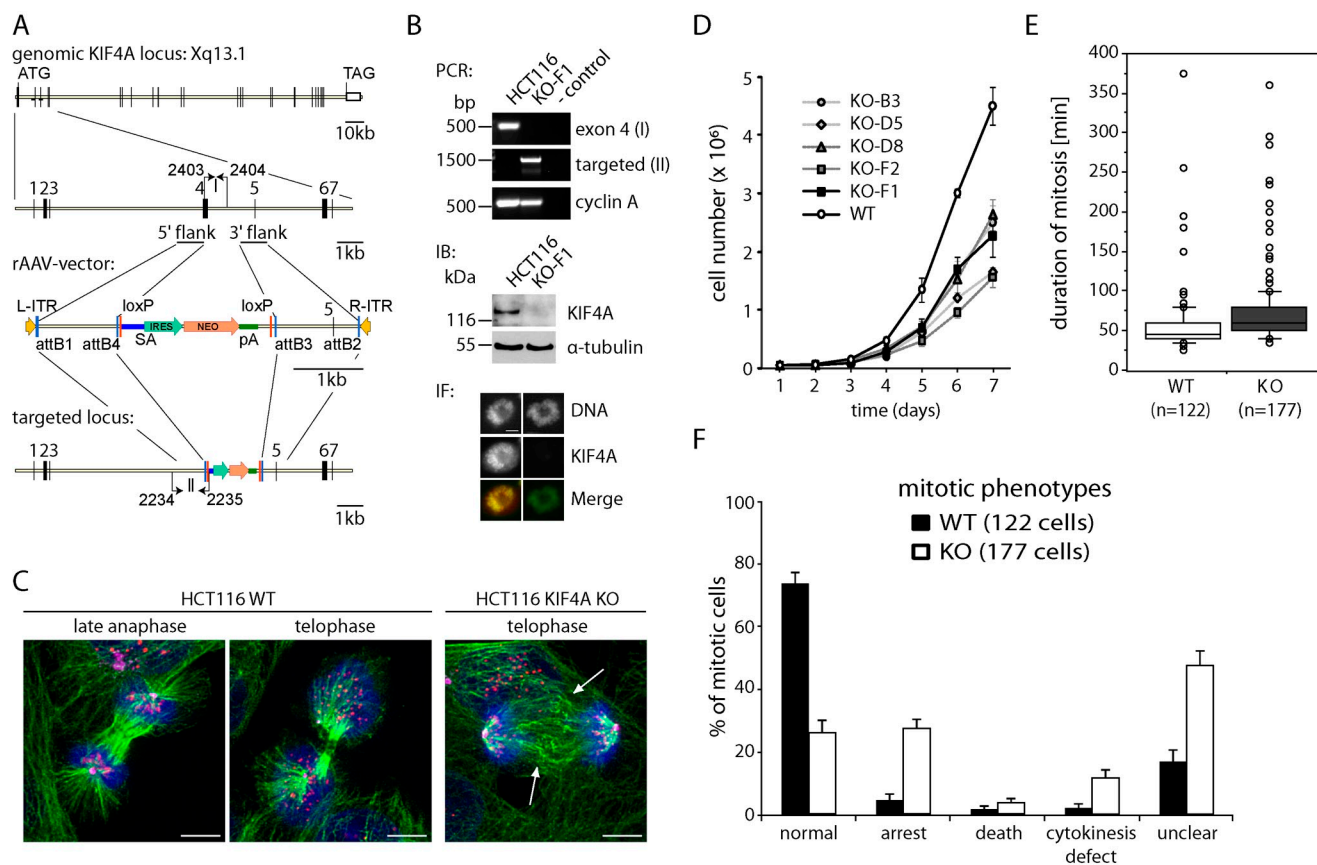
Figure 2. **Generation of a human KIF4A knockout cell line.** (A) Cloning strategy for the generation of a recombinant adeno-associated virus (rAAV) gene targeting construct. (B) HCT116 WT and KIF4A KO clone F1 were analyzed by PCR (top), immunoblotting (middle), and immunofluorescence (bottom), demonstrating correct targeting and the resulting loss of KIF4A protein. (C) HCT116 wild-type and KIF4A KO cells were immunostained for α-tubulin (green), kinetochores (red), pericentrin (pink), and DNA (blue) and confocal z-stacks of anaphase and telophase cells acquired. Deconvolved MIPs are shown. Arrows indicate disorganized midzone MTs. Bar, 5 µm. (D) HCT116 wild-type and five different KIF4A KO clones were seeded at 0.5×10^5 cells per well and cell numbers determined over 7 d. Graphs represent the mean of four independent experiments (±SEM). (E) HCT116 wild-type and KIF4A KO cells were monitored by phase-contrast video live-cell microscopy during a period of 16 h. Mitosis was slightly prolonged in HCT116 KIF4A KO cells as shown in the box-and-whisker plot. (F) Cells from E were classified dependent on their fate during and after mitosis, respectively.

(median: 90 min [$n = 464$]; Fig. S1, A and B) and increased the mitotic index (Fig. 1 B; $17.9 \pm 1.2\%$, P < 0.01). This increase in the mitotic index is likely to be an underestimate due to induction of mitotic cell death in double RNAi cells. When stained for activated caspase 3 48 h after transfection and flow cytometric analysis of cellular DNA content in three independent experiments, cell death was found to be elevated from $1.85 \pm 0.31\%$ in controls to $2.23 \pm 0.26\%$, $3.06 \pm 0.25\%$ and $4.09 \pm 0.75\%$ in hKID, KIF4A, and double chromokinesin RNAi cells, respectively (Table 1).

Spindles in hKID/KIF4A double RNAi cells were elongated (9.94 ± 1.36 µm, $n = 88$), showed wider interkinetochore distances similar to those seen in KIF4A knockdown cells (see following paragraph), and more than 60% of those spindles contained at least three uncongressed chromosomes (Fig.1, D and E). Live-cell imaging revealed that in cells depleted of both chromokinesins, the majority of chromosomes reached the metaphase plate and only a few chromosomes remained uncongressed and close to the spindle poles (Videos 1–4 show examples of control, single, and double RNAi cells). During the prolonged mitosis caused by double chromokinesin knockdown, spindles started to rotate and frequently disintegrated, followed

by the loss of an organized metaphase plate (Fig. S1 A; Video 4), reminiscent of "cohesion fatigue" in prolonged mitoses (Daum et al., 2011; Stevens et al., 2011). The mitotic checkpoint proteins Mad2 and BubR1 were present on kinetochores of unaligned chromosomes (Fig. S2), suggesting that attachment errors cause the alignment failure. Mitotic checkpoint-mediated arrest in hKID/KIF4A RNAi cells was further confirmed by additional knockdown of Mad2 (95% knockdown efficiency), which overcame the chromokinesin RNAi-induced mitotic arrest (Fig. S2 C).

To rule out that the observed KIF4A phenotype was incomplete, we disrupted the KIF4A gene in HCT116 cells by gene targeting using adeno-associated virus for delivery of a gene trap (Fig. 2 A), which resulted in a complete KIF4A knockout as determined by immunoblotting and staining (Fig. 2 B). KIF4A knockout cells proliferated slower than wild-type cells (Fig. 2 D) and lacked an organized spindle midzone (Fig. 2 C), but displayed only a mild increase in bi-nucleated cells as a consequence of cytokinesis failure (Fig. 2 F). KIF4A knockout cells showed disorganized MTs similar to the ones we had observed in KIF4A knockdown HeLa cells (Fig. 3 A, arrows), had a disorganized metaphase plate, and displayed statistically
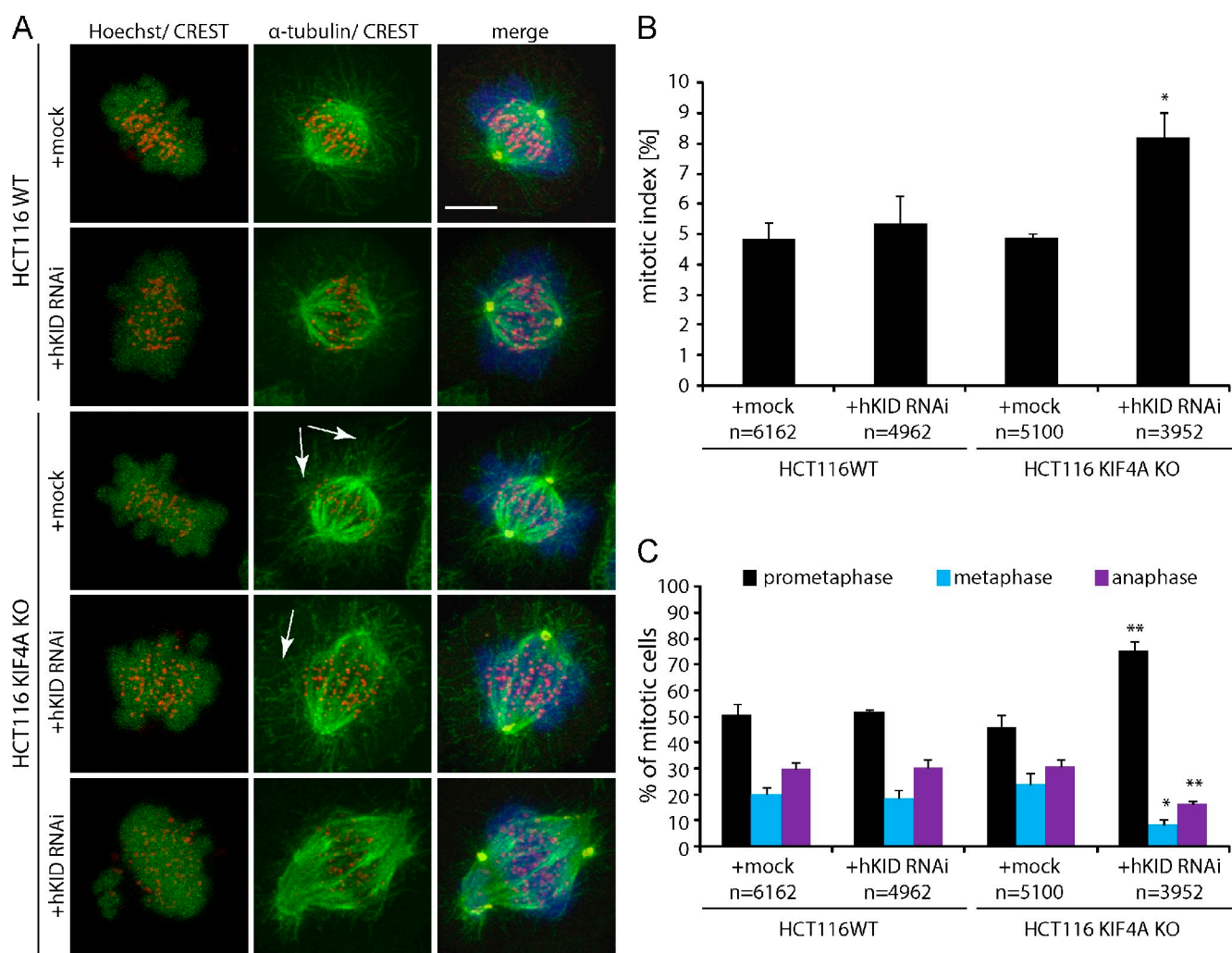
Figure 3. **HCT116 KIF4A knockout cells show mitotic delay after depletion of hKID.** (A) Selected spindles of HCT116 wild-type and KIF4A KO cells after treatment with mock or hKID-siRNA. Shown are MIPs of deconvolved confocal z-stacks. Arrows indicate aberrant nonkinetochore MTs in KIF4A KO cells. Bar, 5 µm. (B) HCT116 wild-type or KIF4A KO cells were transfected with 50 nM mock or hKID-siRNA, methanol-fixed 40 h pt, and stained for DNA. Mitotic index and mitotic phases of four independent experiments + SEM are shown in B and C, respectively. *, Student's *t* test value P < 0.05; **, P < 0.01.

significant (P < 0.05) wider interkinetochore distances (mean ± SEM: 1.34 ± 0.03 µm in knockout cells [*n* = 99 kinetochores] as compared with 1.21 ± 0.03 µm in parental HCT116 cells [*n* = 75] in three independent experiments). Progression through mitosis, however, was only slightly affected (Fig. 2 E).

To investigate whether hKID affects chromosome congression in cells lacking KIF4A, we performed siRNA transfection experiments. Although depletion of hKID in HCT116 wild-type cells did neither affect the mitotic index nor the length of different mitotic phases, hKID RNAi in KIF4A knockout cells lengthened mitosis and increased the frequency of prometaphase cells (Fig. 3, B and C). Thus, the chromokinesin RNAi phenotype could be observed in two different cells lines and by using two different experimental approaches. Our data show that the combined loss of function of hKID and KIF4A is much stronger than the depletion of the individual chromokinesins. Loss-of-function phenotypes of the individual chromokinesins, however, are rather different, suggesting that these two kinesins might carry out different functions that contribute independently to chromosome congression.

hKID/KIF4A RNAi affects chromosome congression

To characterize why and how chromosome congression is disturbed in chromokinesin knockdown cells, we established a high resolution imaging protocol. Chromosome congression was normal in mock (12 of 13 cells; Video 5) and KIF4A-depleted cells (four of five cells, Video 7). Knockdown of hKID had also only a small effect on congression and was normal in three of four cells (Video 6), but chromosomes displayed prominent misorientation of their arms, which pointed toward the pole rather than being perpendicular to the spindle axis. Depletion of both chromokinesins, however, clearly affected chromosome congression because none of the 13 analyzed cells managed to form a proper metaphase plate within the observation period of 30 min (see Videos 8–10). All of these mitoses, which were analyzed by 3D reconstructions of deconvolved z-stacks over time, were characterized by the presence of chromosomes that failed to align at the metaphase plate and whose arms abnormally pointed toward the poles. These chromosomes were clustered, trapped at the poles while their arms appeared to
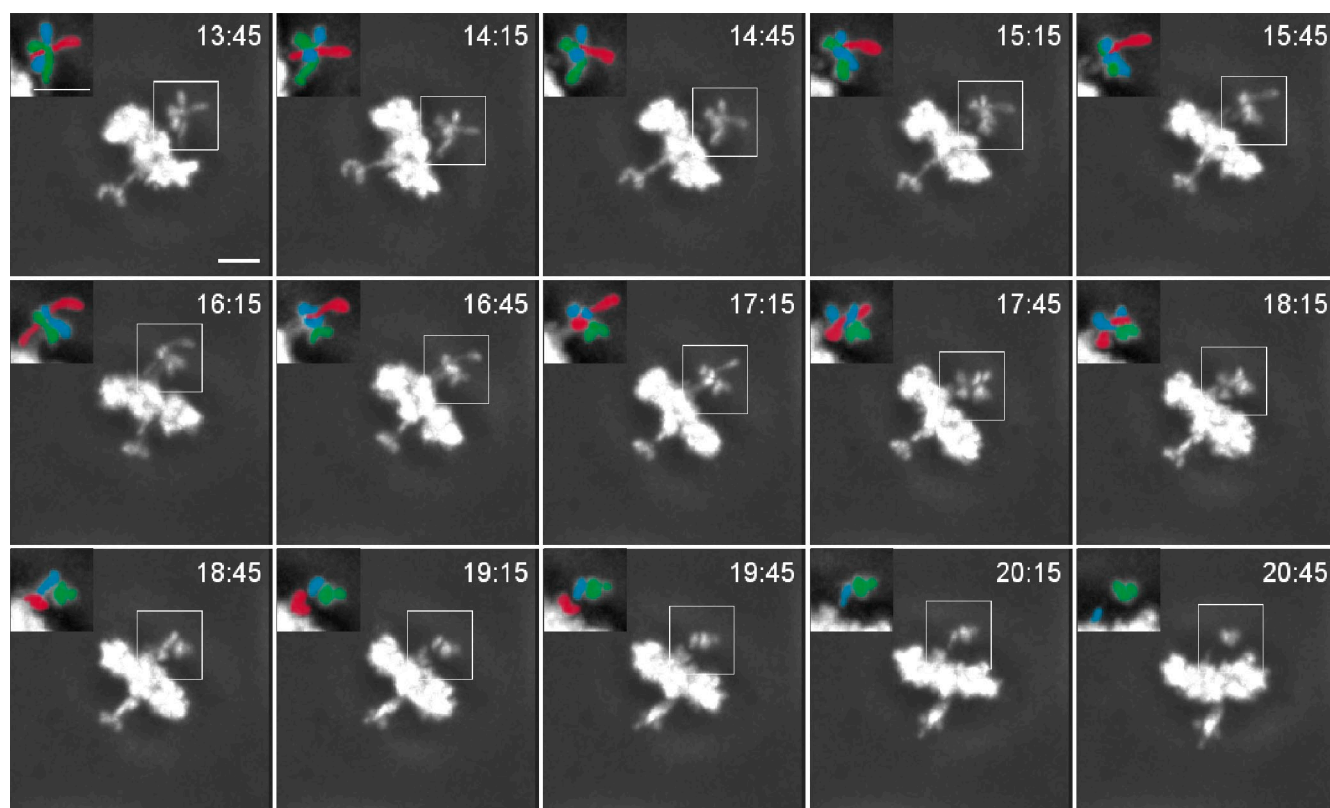
Figure 4. **Loss of chromokinesins causes misorientation and entanglement of chromosome arms.** Selected frames from 4D fluorescence microscopy time-lapse sequence of HeLa H2B-GFP cells 30 h after hKID/KIF4A siRNA transfection. 30 z-sections were taken every 15 s (for a total time of 30 min), processed by deconvolution, and carefully analyzed in 3D over time using Imaris to distinguish different chromosomes. The first frame shows a cell with unaligned chromosomes stuck at the poles. The white box indicates the area of the inset with three chromosomes, labeled in blue, red, and green. The following frames show that these chromosomes remain stuck although their arms get extended as if pulled from the opposite spindle pole. Only after a long delay, the red chromosome becomes free and congresses to the metaphase plate. Time is min:s. Bar, 5 µm.

be entangled (see color-marked chromosomes in Fig. 4) and stretched, reflecting their resistance to the pulling forces from the opposite spindle pole (as can be seen in Videos 8–10). The misorientation of chromosome arms was further confirmed by confocal microscopy (Fig. S3, arrows). A similar, although much weaker, effect was seen in hKID knockdown cells, but not in KIF4A or control knockdowns. These experiments show that hKID RNAi mainly affected the orientation of chromosome arms, whereas chromosome congression was strongly affected only when KIF4A was codepleted.

### Loss of chromokinesins affects chromosome oscillation and kinetochore dynamics

The analysis of KIF4A knockdown HeLa cells during mitosis revealed a broadening of the metaphase plate and an increased interkinetochore distance in methanol fixed cells from 1.10 ± 0.04 µm in controls to 1.38 ± 0.06 µm in KIF4A-depleted cells ($P < 0.05$, mean $\pm$ SEM of three experiments; 3–4 cells and 20 kinetochore pairs analyzed per experiment). To dissect kinetochore dynamics in more detail, we performed RNAi experiments in HeLa CenpA-EGFP cells (Amaro et al., 2010; Jaqaman et al., 2010), which confirmed a wider average interkinetochore distance in living cells (1.01 ± 0.08 µm in controls [$n = 51$], 1.27 ± 0.09 µm in KIF4A RNAi cells [$n = 47$],

$P < 0.001$; Fig. 5 A, Table 1). The distance between sister kinetochores in KIF4A and double chromokinesin RNAi cells was dynamic and hyperstretching was followed by a return to normal interkinetochore distances, excluding loss of sister chromatid cohesion as an explanation.

In control cells, sister kinetochores moved in synchrony with each other and, upon switching, the trailing kinetochore followed the leading one (Fig. 5 B). Similar results were obtained in cells depleted from hKID, although oscillations became slightly slower (Fig. 6, D and E; Table 1) and slightly less regular, as shown by kinetochore cross-correlation analysis (Fig. 6, B and E). In KIF4A knockdown cells, however, we noted that sister kinetochores often moved in different directions (Fig. 5, B and C; arrows highlight aberrant sister kinetochore movements), suggesting a lack of synchrony. To quantify these changes, kinetochores were recorded over a time interval of 5 min from 15 to 20 cells per experiment (three independent experiments). The dynamics of kinetochores in the metaphase plate of mitotic cells were analyzed by measuring the oscillation of kinetochore pairs around a fitted metaphase plate as well as the changes of interkinetochore distances over time ("sister kinetochore breathing"; Amaro et al., 2010; Jaqaman et al., 2010).

To represent the amplitude of kinetochore oscillations, we analyzed the distribution of the sister kinetochore center position
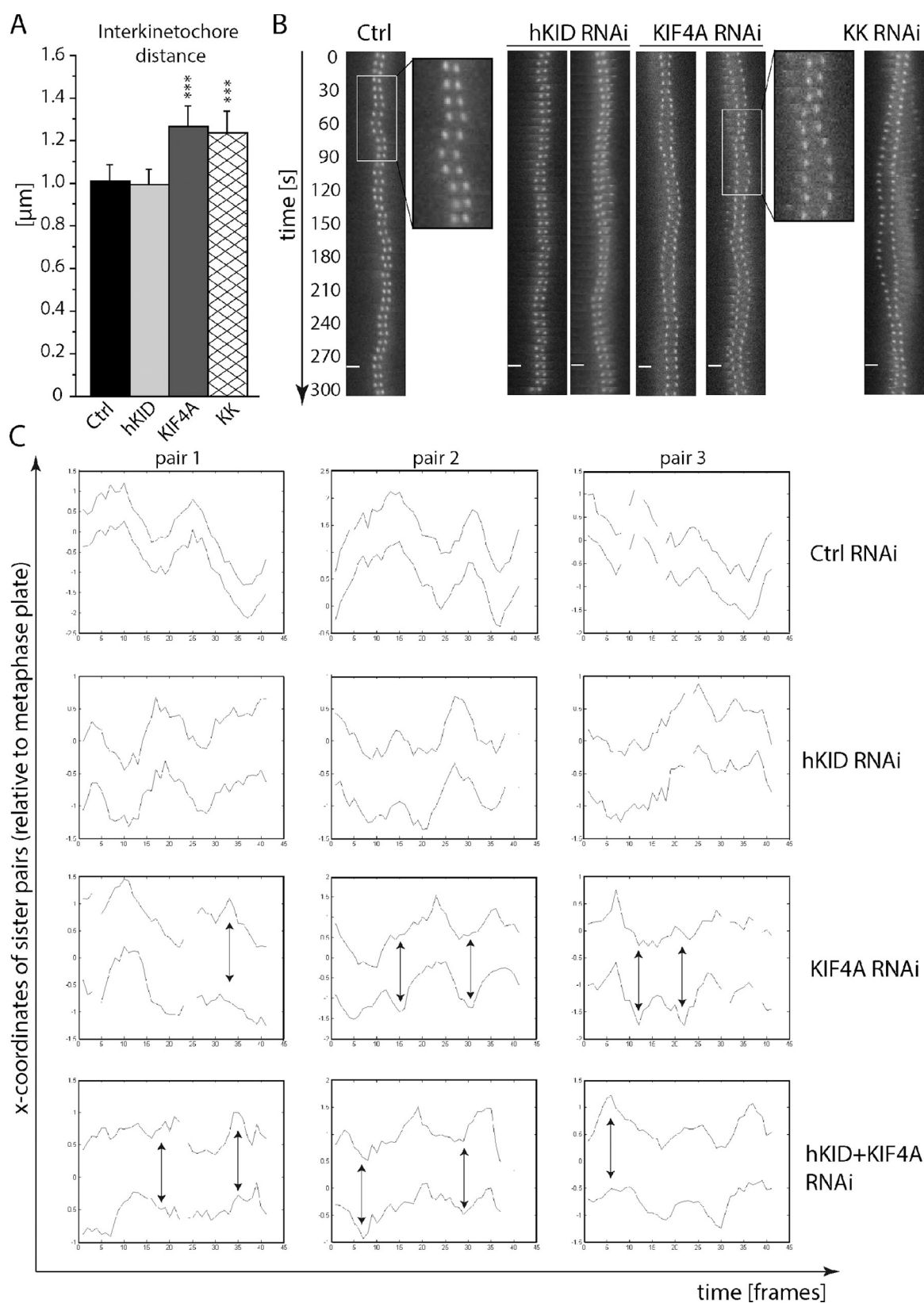
Figure 5. **Loss of hKID and KIF4A induces irregular chromosome oscillations.** HeLa CenpA-EGFP cells were transfected with 50 nM siRNA targeting hKID, KIF4A, or both and imaged 40 h pt. Three independent live-cell imaging experiments were performed for each siRNA treatment. Kinetochore behavior and dynamics were determined using MaKi software. (A) Interkinetochore distance was analyzed from cells of three independent experiments. Columns represent mean + SD. (B) Time-lapse movie frames of kinetochore pairs of control (mock transfected), hKID, KIF4A, and KK siRNA-transfected cells. Boxes show enlarged views of kinetochore pairs. Bar, 2 μm. (C) Oscillatory movements of selected sister pairs after different siRNA treatments were plotted against time (in frames; one frame is 7.5 s). Shown are the x-coordinates of each sister relative to the metaphase plate. Arrows indicate irregular breathings. ***, Student's *t* test value P < 0.001.
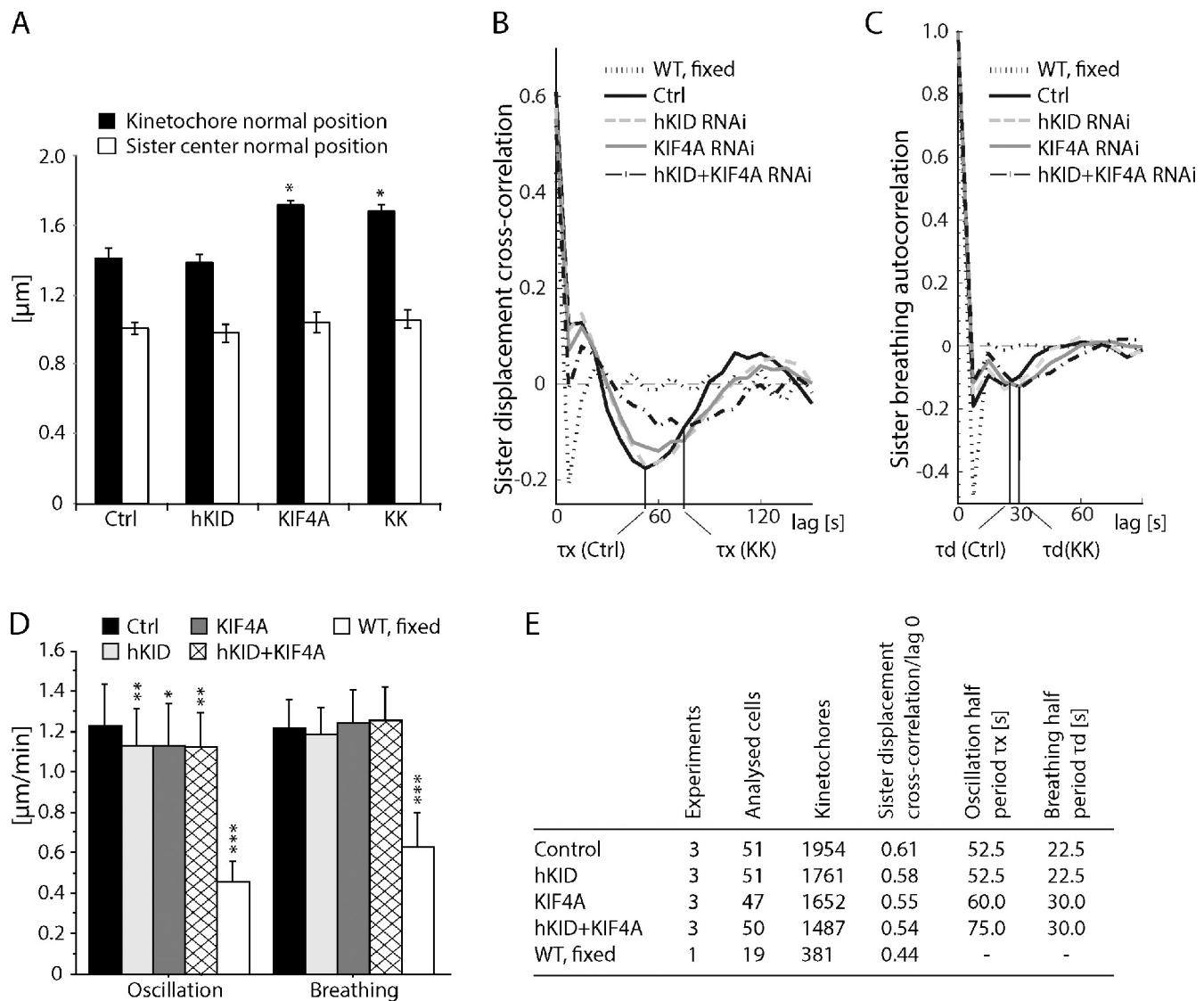
Figure 6. **Loss of KIF4A increases sister separation and prolongs the breathing period.** (A) Kinetochore distribution across a fitted metaphase plate was determined by measuring the sister center position and kinetochore positions. Both values are displayed as the twofold standard deviation of the mean ± SD. (B and C) Dynamic parameters were determined by calculating the sister displacement cross-correlation (B) and sister kinetochore autocorrelation values (C). Methanol-fixed wild-type cells (gray, dashed line) were used as negative control. (D) Oscillation and breathing speed for different siRNA treatments. Columns represent mean + SD. (E) Table summarizing the kinetochore oscillation parameters. *, Student's t test value $P < 0.05$; **, $P < 0.01$; ***, $P < 0.001$.

	Experiments	Analysed cells	Kinetochores	Sister displacement cross-correlation/lag 0	Oscillation half period τx [s]	Breathing half period τd [s]
Control	3	51	1954	0.61	52.5	22.5
hKID	3	51	1761	0.58	52.5	22.5
KIF4A	3	47	1652	0.55	60.0	30.0
hKID+KIF4A	3	50	1487	0.54	75.0	30.0
WT, fixed	1	19	381	0.44	-	-

relative to a fitted metaphase plate and displayed them as the twofold standard deviation. Although the position of the center between the kinetochore pairs across the fitted metaphase plate was not significantly altered under all experimental conditions, the position of individual kinetochores (kinetochore normal position) was significantly increased in KIF4A RNAi cells (Fig. 6 A), consistent with the observed widening of the metaphase plate as observed in fixed and stained cells (Fig. 1 D).

Because the above results suggested that knockdown of hKID and KIF4A had different effects on chromosome oscillations, we analyzed the amplitude and frequency of kinetochore oscillations across the fitted metaphase plate. First, we determined the sister kinetochore cross-correlation values and plotted them as a function of time. As can be seen in Fig. 6, B and E, the sister displacement cross correlation at lag = 0 s, which represents

the synchrony of movements, was reduced from 0.61 in control cells (1,954 kinetochores analyzed in 51 cells in 3 independent experiments) to 0.55 in KIF4A RNAi cells (1,652 kinetochores in 47 cells in 3 independent experiments), similar to values seen in hCAPD2 condensin subunit RNAi cells (Jaqaman et al., 2010), confirming the visual impression of reduced synchrony in sister kinetochore movements. The oscillation half period, τx, was only slightly increased from 52.5 s in control and hKID RNAi cells to 60 s in KIF4A RNAi cells (Fig. 6 D; Table 1). Combined knockdown of hKID and KIF4A, in contrast, resulted in a further loss of synchrony and a strong increase in the oscillation period of sister kinetochore movements ($\tau x = 75$ s in double chromokinesin knockdown cells). Oscillation speed was slightly but significantly reduced upon knockdown of either chromokinesin or both (Fig. 6 D; Table 1). In agreement with a
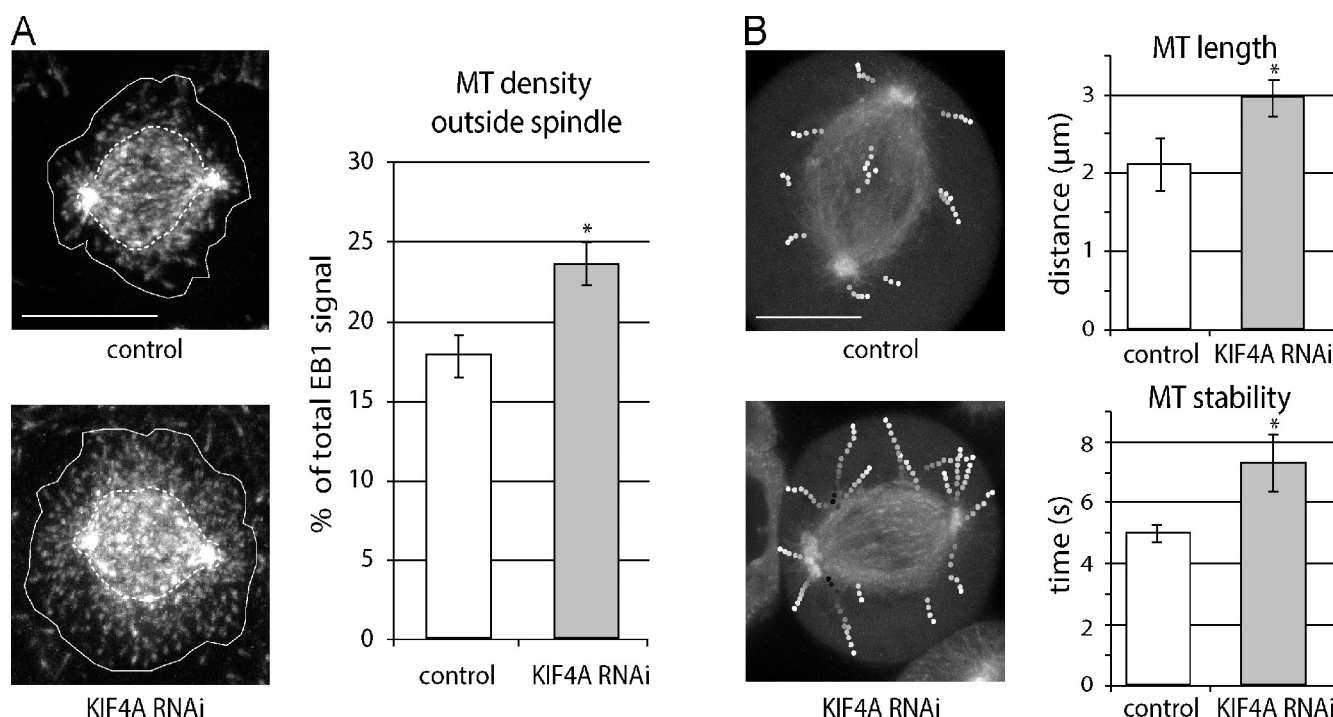
Figure 7. **Loss of KIF4A decreases MT dynamics.** (A) HeLa cells were transfected with KIF4A RNAi or mock, stained for EB1 and kinetochores (CREST antiserum) and imaged by confocal microscopy. Representative maximum intensity projections are shown. Bar, 10 µm. (B) HeLa EB1-GFP cells were transfected with either KIF4A siRNA or mock and imaged 36 h pt. MT plus-ends, marked by EB1, were followed over several frames and MT length and stability were calculated. Bar, 5 µm. Shown is mean of three independent experiments ± SEM.

recent report (Wan et al., 2012), the sister kinetochore breathing period, τd, was about half the oscillation frequency and mirrored the results of cross-correlation analysis

In summary, in contrast to previous observations, we found that chromosome oscillations were not abolished but slower and slightly less regular in hKID RNAi cells. The cross-correlation curves of control, hKID, and KIF4A RNAi cells looked similar to each other whereas knockdown of both chromokinesins were markedly different from the single chromokinesin RNAi cells, indicating a strong loss of regular kinetochore movements in these cells.

KIF4A controls MT dynamics in mitosis

The above experiments demonstrate that knockdown of KIF4A caused more irregular kinetochore movements, which can be caused by alterations in the elasticity of centromeric heterochromatin or by changes in the dynamic behavior of kinetochore MTs (Jaqaman et al., 2010). KIF4A RNAi has been reported to reduce the amount of condensin complexes along chromosome arms (Mazumdar et al., 2004), which could affect the elastic properties of centromeric heterochromatin. However, in our hands neither siRNA-mediated knockdown nor knockout of KIF4A affected the recruitment of condensin complexes to mitotic chromosomes as measured by SMC2 staining (unpublished data). Thus, how KIF4A interacts with condensin complexes is still unclear and further experiments are required to clarify this important issue.

To investigate the second hypothesis, we had a closer look at MTs in control and KIF4A knockdown and knockout cells. First, we evaluated whether KIF4A depletion resulted in MT

destabilization and determined K-fiber abundance after cold treatment (Rieder and Borisy, 1981). As can be seen in Fig. S4 D, no change in K-fibers could be seen in KIF4A RNAi cells, which excludes a strong destabilizing effect of KIF4A depletion of MTs. In immunostaining experiments we noticed, however, that KIF4A-depleted cells had longer and/or abnormal MTs than control cells (Figs. 1 D and 3 A). To investigate the role of KIF4A on MTs in human mitosis, we generated a HeLa cell line stably expressing EB1-GFP to facilitate measurements of MT dynamics by MT plus-end tracking. First, we fixed HeLa EB1-GFP cells 36–48 h after transfection with control and KIF4A siRNAs and analyzed them by confocal microscopy. As can be seen in Fig. 7 A and Table 1, KIF4A knockdown cells displayed an increase in MT plus-ends outside the area of the mitotic spindle, confirming the results obtained by tubulin immunofluorescence staining experiments shown above. When EB1-GFP and additionally EB3-YFP signals were monitored by live-cell confocal imaging of mitotic HeLa cells, we noticed that in KIF4A-depleted cells, the labeled MT plus-ends could be tracked over longer distances and for extended periods of time (Fig. 7 B; Fig. S4, A–C; Table 1) compared with control RNAi cells. Because this increase in number and length of MTs upon knockdown of KIF4A could affect the PEF, we measured the radial position of chromosomes in monopolar spindles. Therefore, HeLa cells stably expressing α-tubulin–mRFP and EGFP-centrin1 were treated with 100 µM monastrol for 3 h after knockdown of chromokinesins and stained for the outer kinetochore marker HEC1. Z-stacks of monopolar spindles were acquired and the distance between kinetochores and the closest centriole was determined. In control cells, the average distance was 3.98 ± 0.08 µm,
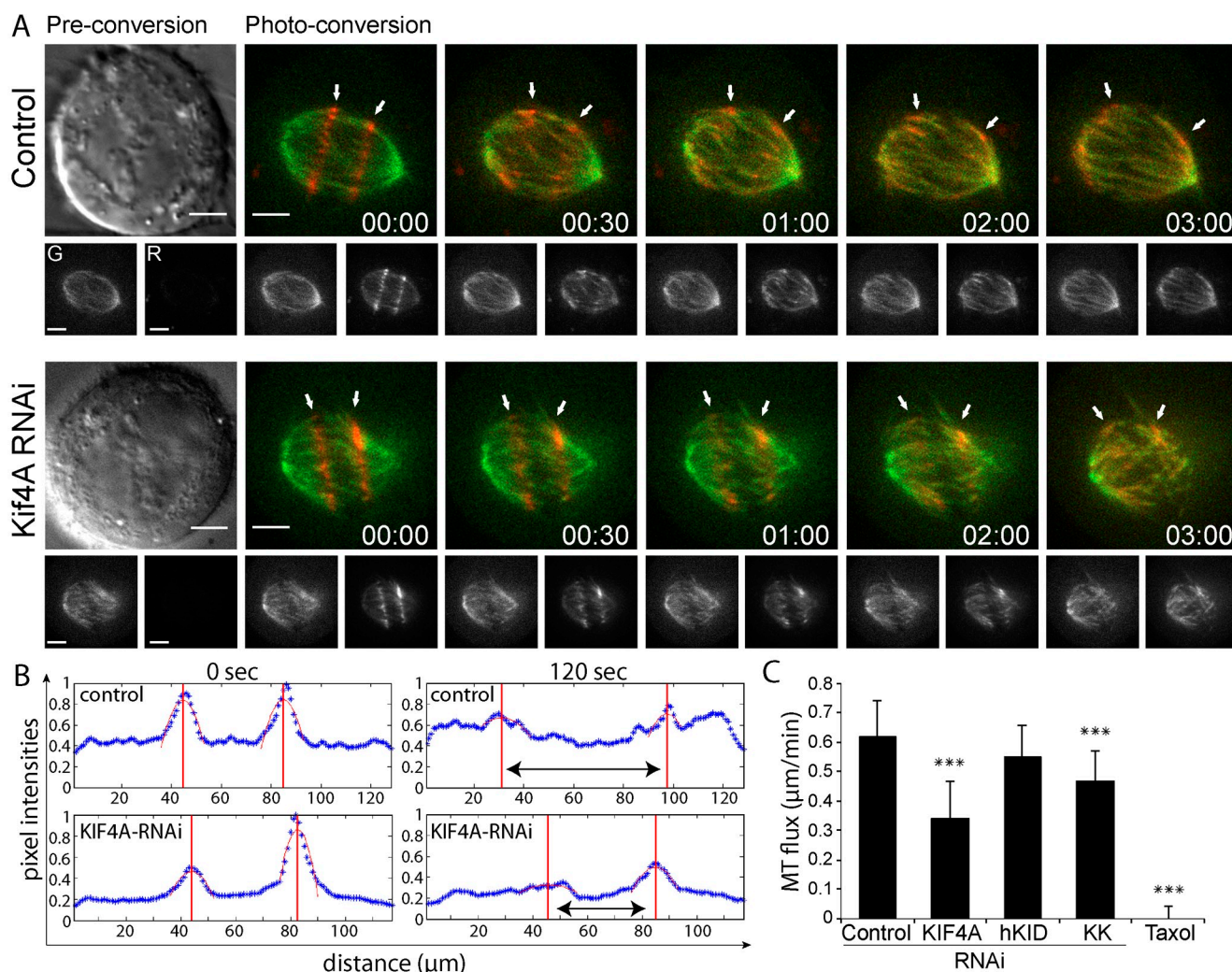
Figure 8. **Loss of KIF4A decreases MT flux.** (A) DIC and fluorescence images show representative control and KIF4A-depleted cells in late prometaphase/metaphase. Images were captured before (preconversion) and at various time points (indicated in minutes and seconds) after photo-conversion of mEos-α-tubulin. MT flux was measured by photo-conversion of regions from both half-spindles in U2OS-mEos-tubulin cells and photo-converted mEos-tubulin was tracked over a time interval of 3 min (arrows). Bottom panels of each merged frame show separated green and red channels. Bar, 5 μm. (B) Representative fluorescence intensity curves of control vs. KIF4A-depleted U2OS-mEos-tubulin cell created immediately after photo-conversion and 120 s later. Fluorescence intensity peaks are generated by manual estimation of the peak region, followed by fitting of the intensity data points to a parabola. The maximum of the parabola was used as the effective peak position. (C) Both KIF4A and KIF4A/hKID double-knockdown late prometaphase/metaphase U2OS-mEos-tubulin cells display significant reduction of kinetochore-MT poleward flux in comparison with controls (P < 0.001). Error bars represent SEM derived from three independent experiments each containing 11–26 cells.

which was reduced to 3.12 ± 0.11 μm upon hKID knockdown, similar to values reported previously (Tokai-Nishizumi et al., 2005; Santamaria et al., 2008; Stumpff et al., 2012). A similar reduction could be seen after depletion of both chromokinesins (2.85 ± 0.06 μm), whereas the average distance of chromosomes from the closest centriole in KIF4A-depleted cells was only slightly reduced to 3.78 ± 0.06 μm. Thus, KIF4A controls the length of MTs in mitosis but this effect does not impact strongly on PEFs, which are mainly generated by hKID (Fig. S4 E; Table 1).

Next, we measured MT turnover and flux rates in mitotic U2OS cells stably expressing α-tubulin fused to the photoconvertible fluorescent protein mEos2 (McKinney et al., 2009). For measuring flux rates by photo-conversion, two bar-like regions—one on each side of the metaphase plate—were selected

within the mitotic spindle, converted from green to red fluorescence by pulsed UV-irradiation, and followed over time. The increasing distance between those bars was used to calculate MT flux (Fig. 8, A and B; Table 1). Interestingly, we found that knockdown of KIF4A significantly decreased flux from 0.62 ± 0.12 μm/min in mock-transfected cells to 0.34 ± 0.13 μm/min (mean of three independent experiments ± SEM; P < 0.001; Fig. 8 C). Knockdown of hKID did not slow down flux (0.55 ± 0.11 μm/min), whereas depletion of both hKID and KIF4A decreased flux similarly to the knockdown of KIF4A alone (0.47 ± 0.10 μm/min). Using this photo-conversion assay, we also measured the decay rate of photo-activated mEos-tubulin over time, which fitted very well to a double exponential function (coefficient of determination R^2 > 0.99 in all cases) containing fast and slow fluorescence decay rates, consistent with an initial

rapid decay (see Fig. S5 A) and a later slower decay rate (see Materials and methods). The half-life of MTs extracted from these decay rates was similar (∼2 min for kinetochore MTs and 12 s for nonkinetochore MTs; Fig. S5 B) under all experimental conditions, suggesting that loss of KIF4A did not control the overall turnover of MTs but had a selective effect on MT flux.

Discussion

In agreement with previous studies, we confirm here that hKID is the major mediator of the PEF (Levesque and Compton, 2001; Brouhard and Hunt, 2005; Bieling et al., 2010a; Stumpff et al., 2012) and demonstrate that hKID becomes important for chromosome alignment after codepletion of KIF4A. PEFs were found to control the probability of switching from poleward (P) to antipoleward (AP) movements, and reduction of PEFs by laser-mediated chromosome arm–cutting experiments or hKID RNAi resulted in wider and aberrant chromosome oscillations (Ke et al., 2009; Stumpff et al., 2012). Switches in chromosome movements are induced by kinetochore tension and result from changes in kinetochore MT dynamics (Kapoor and Compton, 2002). A switch in chromosome movement could, therefore, reflect a correction mechanism sensing an abnormal chromosomal position, i.e., too close to the spindle pole, facilitating chromosome congression to the metaphase plate. Our analysis, however, showed that hKID depletion has only little influence on the oscillation of congressed metaphase chromosomes, suggesting that PEFs mainly influence the movements of noncongressed chromosomes. When the kinetochore MT stabilizing kinesin KIF18A, a major regulator of chromosome alignment, was codepleted along with hKID, chromosome alignment was severely impaired, yet oscillations still continued (Stumpff et al., 2012). These experiments suggested that reliable chromosome alignment at the metaphase plate requires a MT length-dependent MT stabilizer, e.g., KIF18A (Stumpff et al., 2008), as well as a force generator, e.g., hKID, that pushes chromosomes toward, and keeps them close to, the cellular equator. Thus, hKID appears to become essential whenever MT dynamics or bipolar spindle formation are perturbed by other means, e.g., by treating cells with low doses of nocodazole, codepletion of KIF4A or KIF18A (Stumpff et al., 2012), or by inhibition of NUMA (Levesque et al., 2003).

On congressed chromosomes, hKID is required to straighten out chromosome arms perpendicular to the spindle axis as a consequence of the two PEF vectors (Rieder et al., 1986). The assembly of chromosomes in a toroid with radially outward pointing arms has been shown to be important for the rapid conversion of initial lateral to stable end-on attachments to avoid erroneous attachments and segregation errors (Magidson et al., 2011). Consistent with the functions of hKID in promoting microtubule attachments, we noted that prometaphase is prolonged in hKID-depleted cells.

Compared with controls, mitotic spindles in KIF4A-depleted cells appeared to have more MTs, in particular, astral MTs. This finding is consistent with the observed increase in MT density of in vitro spindles assembled in Xklp1-depleted conditions (Castoldi and Vernos, 2006; Bieling et al., 2010a). Xklp1 was shown to stabilize MTs by slowing down their

polymerization as well as depolymerization rate (Bringmann et al., 2004) and Xklp1 depletion was found to lengthen MTs in vitro (Castoldi and Vernos, 2006), whereas KIF4A has been shown to control MT length during anaphase and telophase (Kurasawa et al., 2004; Zhu and Jiang, 2005; Bieling et al., 2010b; Hu et al., 2011, 2012). By staining MTs in KIF4A knockdown cells, we noticed that also metaphase mitotic spindles looked more disorganized than in control cells. Like Xklp1-deficient spindles assembled in vitro (Castoldi and Vernos, 2006), spindles of KIF4A-depleted somatic cells in vivo displayed an altered shape and seemed to contain more MTs. These findings suggest that KIF4A normally limits MT elongation and thereby contributes to the density of MT plus-ends in the vicinity of chromosomes. Microtubule density could support hKID to generate the PEF. Consistent with this hypothesis, but in contrast to Stumpff et al. (2012), who reported a slight increase in the radial distance of chromosomes after knockdown of KIF4A in HeLa cells, we saw a small although statistically not significant shrinkage of monopolar spindles, a finding that would be in line with the role of KLP-19 in generating PEFs in *C. elegans* (Powers et al., 2004). A potential contribution of KIF4A to PEFs thus deserves further evaluation in human cells.

Using plus-end tracking and photo-conversion experiments, we found that MTs were longer due to increased lifetime in KIF4A RNAi cells, showing that KIF4A also controls MT dynamics in early mitosis. During the revision of our manuscript, it was reported that depletion of KIF4A stabilized MTs by promoting MT polymerization (Stumpff et al., 2012). Our tracking data confirm this finding; however, as we did not see an increase in MT polymerization rate, we suggest that the increased MT stability may result from a decrease in MT catastrophes.

In addition to slowing down MT dynamics, knockdown of KIF4A caused irregular chromosome oscillations, which, in contrast to the findings of Stumpff et al. (2012), led to a disorganized metaphase plate. Currently, there are three possible explanations for this observation: (1) KIF4A has an important function on chromosome structure that is required for chromosome motility, (2) KIF4A cooperates with hKID to generate the PEF that contributes to chromosome movements, and (3) KIF4A has another function on spindle MTs, e.g., as a force equalizer, that affects kinetochore MT behavior and, thus, chromosome dynamics.

The first hypothesis is supported by the fact that KIF4A has been shown to affect condensin loading onto chromosomes (Mazumdar et al., 2004), and the changes that we observed in our analysis of kinetochore oscillations are very similar to those seen in condensin subunit–depleted cells (Ribeiro et al., 2009; Jaqaman et al., 2010). We could not, however, detect any differences in condensin loading on mitotic chromosomes of KIF4A knockdown or knockout cells (unpublished data) and did not, therefore, investigate the postulated link between KIF4A-induced changes in centromeric chromatin compaction and altered chromosome oscillations. The fact that KIF4A depletion weakens centromeric cohesion, causes irregular chromosome movements and reduces MT flux, points to a role of KIF4A on kinetochore function that needs to be further investigated. The second hypothesis is supported by experiments demonstrating
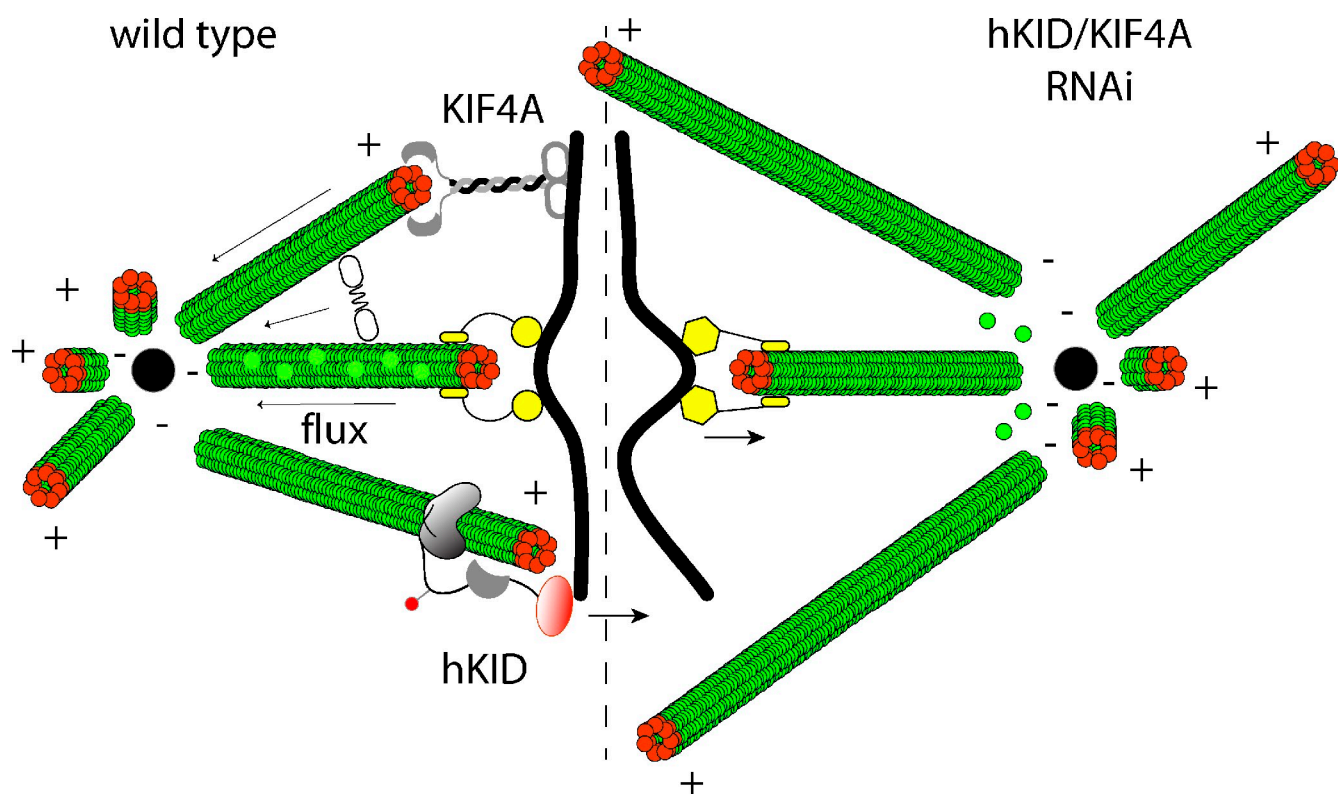
Figure 9. **Model for chromokinesin function in chromosome congression.** The left-hand side of the scheme depicts the proposed functions of hKID and KIF4A. On aligned chromosomes, hKID stabilizes the orientation of chromosome arms and by generating PEF that pushes the spindle poles apart. KIF4A limits the elongation of MTs near chromatin and could thereby control the number of MT plus-ends interacting with chromosomes or with MTs from the opposite pole (sliding interpolar MTs). Via MT cross-linking proteins MT-dependent forces are distributed throughout the spindle, which is required for regular chromosome oscillations. Reduced kinetochore MT flux after loss of KIF4A could either be due to changes in the dynamics of MTs interacting with chromosome arms or could be caused by a tighter binding of MTs to kinetochores due to kinetochore stretching (yellow symbols). In combination with loss of hKID, this results in chromosome attachment, congression, and segregation failures.

that both chromokinesins are required to mediate the interaction of MTs with chromatin (Bieling et al., 2010a). Compared with hKID, KIF4A has a very limited effect on the PEFs (Brouhard and Hunt, 2005; this paper) and some of its functions require hKID (Stumpff et al., 2012). Thus, if KIF4A only acts to support hKID, then, unlike we observed, their combined knockdown should be similar to the knockdown of hKID alone.

KIF4A, therefore, appears to have an additional function in early mitosis that might impinge directly on chromosome motility and thus may cause the irregular oscillations that we detected in KIF4A RNAi cells. One clue to this still poorly defined function comes from our observation that knockdown of KIF4A was sufficient to reduce MT flux rate by ~50%. Because KIF4A has not yet been detected at kinetochores, it likely exerts its effects on MT flux indirectly, e.g., by affecting centromeric chromatin (see previous paragraph) or by controlling the number/processivity of interpolar sliding MTs, which could, via cross-linking proteins, affect MT flux as suggested by Matos et al. (2009). Similar reductions in flux have been observed previously upon depletion of the KIF4 homologue KLP3A in *Drosophila* S2 cells (Buster and Sharp, 2005). A reduction in kinetochore MT flux by itself has, however, little effect on chromosome oscillation and congression (Ganem et al., 2005), and KIF4A's effect on MT flux may therefore only be an indicator of KIF4A's

function on MT-dependent forces acting within the mitotic spindle, which might result in irregular chromosome oscillations.

Our results on the function of chromokinesins in mitosis are very similar to those obtained by Stumpff et al. (2012) who studied the effect of chromokinesin depletion in KIF18A-depleted cells. Although most of the data are in good agreement with each other, Stumpff et al. (2012) did not see a synergistic effect of hKID and KIF4A depletion on chromosome congression. To exclude nonspecific effects in KIF4A RNAi experiments, we generated a KIF4A-deficient cell line in which hKID RNAi also caused chromosome congression defects. Consistent with our findings, individual knockdown of the kinesin 4 and 10 homologues, Klp3A and Nod, in *Drosophila* S2 cells only slightly affected the formation of normal metaphases, whereas codepletion of both chromokinesins resulted in severe chromosome congression defects (Goshima and Vale, 2003).

In summary, our data show that chromokinesins contribute to chromosome congression via different pathways. hKID provides the ejection force that is required to position the arms of chromosomes properly but is not essential for metaphase plate formation. KIF4A mainly contributes to MT dynamics and both together are required for chromosome congression to the metaphase plate. They most likely act by indirectly exerting different forces on kinetochores that control MT dynamics and

chromosome movements. Fig. 9 summarizes our findings: loss of both hKID and KIF4A results in abnormally long MTs that do not interact with chromosome arms, causes irregular chromosome oscillation and kinetochore stretching, as well as a reduction in kinetochore MT flux. As a consequence of chromokinesin knockdown, chromosomes remain excluded from the metaphase plate and delay mitosis due to the incapacity of satisfying the mitotic checkpoint.

Although hKID and KIF4A are individually not essential for mitosis, they are important for the fidelity of chromosome segregation. Powers et al. (2004) documented that PEFs are essential for chromosome alignment of holocentric chromosomes during the brief prometaphase in nematodes and suggested that chromokinesins could perhaps facilitate the alignment of monocentric chromosomes during the slow mitosis of vertebrates. Consistent with this hypothesis, depletion of KIF4 has been linked to the generation of aneuploidy in mouse cells (Mazumdar et al., 2006). In the future it will be interesting to see whether chromokinesins are involved in human tumorigenesis, as suggested recently (Gao et al., 2011). Further, the development of hKID inhibitors might be clinically useful to enhance the aneuploidogenic, toxic effects of MT-depolymerizing agents such as colchicine or vincristine, important antimitotic agents in cancer therapy.

Materials and methods

Reagents, plasmids, and antibodies

All chemicals were obtained from Sigma-Aldrich, enzymes from Promega, and oligonucleotides from MWG Biotech, unless stated otherwise. To create mEOS2 fusion protein expression vectors, human α-tubulin was excised from EYFP-tubulin (Takara Bio Inc.) and subcloned into pmEOS2-C1 (kindly provided by M.W. Davidson, Florida State University, Tallahassee, FL). For detection by immunoblotting or staining we used an anti-KIF4A rabbit polyclonal antiserum (kindly provided by E.A. Nigg, Biozentrum, Basel, Switzerland) as well as a purified anti-KIF4A rabbit polyclonal antibody that we obtained by immunizing two rabbits with a bacterially expressed and GSH-Sepharose (GE Healthcare) purified recombinant GST-tagged C-terminal KIF4A fragment (aa 1000–1232, KIF4A-GD) and purification against KIF4A-GD, cleaved off GST using 3C-protease. To detect hKID, we used an affinity-purified mouse monoclonal antibody (mAb) 8C12, raised against a bacterially expressed, metal affinity-purified N-terminally hexa-histidine-tagged fragment of hKID, encompassing the C-terminal 250 residues (Wandke and Geley, 2006). In addition, specific antibodies were used to detect α-tubulin (mAb B512, Sigma-Aldrich; rabbit #18251, Abcam; and Tat-1, J. Gannon, Cancer Research UK, South Mimms, UK), acetylated α-tubulin (mAb 611B-1; Sigma-Aldrich), BubR1 (mAb, T. Yen, Fox Chase Cancer Center, Philadelphia, PA), Mad2 (rabbit, R. Benezra, Memorial Sloan-Kettering Cancer Center, New York, NY), HEC1 (mAb 9G3; Abcam), GAPDH (mAb 6C5, HyTest. Ltd.), and Alexa Fluor 488–conjugated rabbit anti-activated capase 3 (#9669; Cell Signaling Technology), as well as anti-centromere–positive human CREST serum (G. Wick, Innsbruck, Austria) for kinetochore staining.

Cell culture, transfection, and retroviral transduction

HeLa, U2OS, HEK293, and HCT116 cells were grown in DME/10% FCS under standard conditions as described previously (Wolf et al., 2006). For live-cell imaging or immunofluorescence staining experiments, cells were grown on glass-bottomed dishes. For transient transfection experiments, Lipofectamine 2000 (Invitrogen) was used according to the manufacturer's protocol; stable transfections were performed by transfecting 2×10^5 cells with AgeI linearized plasmids (pmEOS2-tubulin, pEB1-GFP) using Lipofectamine 2000, followed by selection against 1 mg/ml G418, visual identification of positive clones, and subsequent cloning and expansion (Wolf et al., 2006). HeLa H2B-GFP cells were generated by transducing HeLa cells with a pLIB-derived retrovirus (Takara Bio Inc.), which expresses histone H2B-GFP under the control of the retroviral LTR promoter

(Wolf et al., 2006). HeLa EGFP-CenpA cells (Jaqaman et al., 2010) were cultured in the presence of 0.5 µg/ml puromycin and HeLa tubulin-mRFP EGFP-centrin1 cells (Oshimori et al., 2006; Logarinho et al., 2012) in 0.25 µg/ml puromycin and 0.2 mg/ml G418. The HeLa EB3-YFP cell line was generated using pIRESpuro2-EB3-YFP and cultured in DME/10% FCS containing 0.5 µg/ml puromycin.

RNA interference

HeLa and U2OS cells were transfected at 30–50% confluency using Lipofectamine 2000 (Invitrogen) according to the manufacturer's protocol with 25–50 nM siRNAs targeting hKID (#1: 5′-CAAGCUCACUCGCCU-AUUGTT-3′ [Wolf et al., 2006] and #2: 5′-GAUUGGAGCUACUCGU-CGUTT-3′ [Tokai-Nishizumi et al., 2005]); KIF4A (p1 #4: 5′-GCAAGAUC-CUGAAAGAGAUTT-3′ or #3: 5′-GCAGAUUGAAAGCCUAGAGTT-3′), MAD2 (5′-GAGUCGGGACCACAGUUUAUU-3′; Martin-Lluesma et al., 2002), and firefly luciferase (5′-GCUAUGAAACGAUAUGGGCTT-3′) as control. In all transfection experiments, with less than 50 nM siRNA input, control siRNA was added to 50 nM to avoid transfection artifacts. Time-lapse live-cell imaging experiments monitoring cells for 10–16 h for progression through mitosis started 25 h after transfection. Transfections for monastrol assays were performed using Oligofectamine (Invitrogen) according to the manufacturer's protocol.

AAV-mediated gene targeting

The AAV-based targeting vector was constructed by PCR amplification of ~1 kb genomic HCT116 DNA fragments, which were flanked by attB sites for transfer into ENTR vectors. The 5′ flank and 3′ flank containing ENTR vectors were mixed with an ENTR vector containing the gene trap cassette (kindly provided by F. Bunz, Johns Hopkins University, Baltimore, MD) and an AAV-DEST vector for LR clonase (Invitrogen)–mediated recombination. Recombinant AAV plasmid was transfected in HEK293T cells along with pHelper and pRC (Agilent Technologies) to obtain infectious rAAV particles to infect near diploid male HCT116 cells. 72 h after infection cells were transferred to 96-well plates for limiting dilution in the presence of 0.5 mg/ml G418. Clones were replica plated and analyzed for targeting events by PCR using primers 2334 (5′-TTATGGGTCTTTCTGCAAAC-3′) and 2335 (5′-AGAGCGCCAACTTTGTATAG-3′) and confirmed by using primers 2403 (5′-GAGCAAGAGAATGAACCAAC-3′) and 2404 (5′-AAG-GGAAATCAAACACTCTTC-3′) for the presence or absence of exon 4.

Immunoblotting, fluorescence microscopy, and image processing

Immunoblotting was performed using total cell lysates or protein extracts as described previously (Wolf et al., 2006). Total cell extracts corresponding to 10^4 cells per lane were separated on denaturing polyacrylamide gels and semidry blotted onto nitrocellulose filters. After blocking in 10% nonfat milk/PBS/0.5% NP-40, blots were incubated with primary antibodies diluted in blocking solution overnight at 4°C, washed, incubated with secondary HRP-conjugated antibodies (Dako) for 1 h at RT, and developed using enhanced chemiluminescence (Thermo Fisher Scientific). For immunofluorescence staining, cells were processed as described previously (Wolf et al., 2006). Confocal images were generated on a microscope (TCS-SP5 DMI6000; Leica) equipped with a 405-nm diode, an argon ion, a 561-nm DPSS, and a 633-nm HeNe laser. Images were acquired using an HCX PL APO lambda 63x, NA 1.4 oil UV objective at a pixel resolution of 67 nm (Barisic et al., 2010). Images were converted to 8-bit TIFF format by ImageJ (National Institutes of Health, Bethesda, MD), analyzed using MetaMorph 7.0 (Molecular Devices), and further processed using Adobe Photoshop CS3 and Adobe Illustrator CS3 (Adobe Systems). Image z-stacks were deconvolved using Huygens software (Scientific Volume Imaging).

For determination of the mitotic index, HeLa or HCT116 cells were methanol fixed 40 h after siRNA treatment, DNA was visualized by Hoechst 33342 staining, and cells were imaged on a microscope (Axiovert 200M; Carl Zeiss) using a LD 40x/NA 0.75/Ph2 Plan-Neofluor objective. 20 images (1,200–1,600 cells) were analyzed per experiment and mitotic cells identified in the UV channel by their condensed DNA content.

Live-cell time-lapse imaging

Live-cell microscopy was performed on the Axiovert 200M microscope using a LD 40x/NA 0.75/Ph2 Plan-Neofluor objective with images taken every 5 min over a period of up to 16 h without causing light damage to the cells using a 1300 × 1030 12-bit camera at 10 MHz (Coolsnapfx; Photometrics) controlled by MetaMorph software 7.0. Cells were incubated on the microscope in DME/10% FCS at 37°C in a 5% CO_2-containing atmosphere and media prevented from evaporation by sealing the culture dishes with a gas-permeable Teflon membrane (Wolf et al., 2006). For higher

time resolution, movies were acquired under the described conditions using 1-min frame-to-frame intervals over a period up to 8 h. High resolution four-dimensional imaging was performed using a MetaMorph 7.0 controlled Cascade II camera (512 × 512 EMCCD; Photometrics) with EM gain 3500 and 10 MHz and acquired using a Plan-Apochromat 100x NA 1.3 oil objective, imaging every 15 s (0.5 µm z-interval, 30 z-sections) for a total of 30 min. Light toxicity was minimized by decreasing the fluorescence lamp intensity to 12% and including a neutral density filter. Movies were deconvolved using Huygens and chromosome movements were carefully analyzed using Imaris XT (Bitplane). All movies were analyzed manually and duration of early mitosis was determined as the period between the onset of chromosome condensation (prometaphase) and anaphase onset. Cells were further scored for lagging chromosomes and defective cytokinesis.

To measure kinetochore dynamics, HeLa EGFP-CenpA cells were grown on Lab-Tek II chambers (Thermo Fisher Scientific) and imaged in CO$_2$-independent Leibovitz L-15 medium (Sigma-Aldrich) supplemented with 10% FCS. Time points comprising 30 z-sections 0.5 µm apart were acquired every 7.5 s for 5 min on a DeltaVision microscope (Applied Precision; microscope stand: Olympus) using a 100x NA 1.4 oil UPlanSApo objective and a Coolsnap HQ2 camera (Photometrics). Four-dimensional movies were processed and deconvolved using softWoRx (Applied Precision). Data analysis was performed using MaKi software, written in Matlab (The MathWorks, Inc.) as described previously (Amaro et al., 2010; Jaqaman et al., 2010). Image analysis results were visualized using Imaris XT software (Bitplane).

MT flux, polymerization, and K-fiber stability

Photo-conversion experiments were performed using a stable U2OS-mEos-tubulin cell line cultivated on glass-bottomed dishes (MatTek Corporation). Imaging was performed using a 100x 1.4 NA Plan-Apochromat DIC objective on an inverted microscope (TE2000-U; Nikon) equipped with a CSU-X1 spinning-disk confocal head (Yokogawa Corporation on America) provided with two laser lines (488 nm and 561 nm), a Mosaic photo-activation system (Andor Technology) also provided with two laser lines (405 nm and 488 nm), and an iXonEM+ EM-CCD camera (Andor Technology). Late prometaphase/metaphase cells were identified upon green fluorescent tubulin signals and two thin rectangular regions of interest were placed perpendicular to the main spindle axis on both sides of the metaphase plate in order to be photo-activated. Photo-conversion was performed by one 500-ms pulse from a 405-nm laser. Photo-converted red signals were then followed over time together with green fluorescence signals using 561- and 488-nm lasers and images were acquired every 1 s for 3 min.

MT flux was quantified by tracking photo-converted mEos-tubulin over time using an algorithm written in Matlab programming language. At each time frame the position of the photo-activated region was first visually estimated, after which the algorithm performed a parabolic fit to the intensity values in the neighborhood of the estimated position. Measured distances between peaks over time were then used to calculate the average MT poleward velocity by linear fitting.

MT turnover was quantified by measuring integrated pixel intensities within an area enclosing the stripe. To compensate for poleward motion of the stripe we performed a prealignment of the kymograph. This was done by shifting each time-slice of the kymograph by an amount corresponding to the shift (relative to the first frame) of the center of mass of the stripe. To attenuate the effect of noise on center-of-mass calculations that may occur at a number of time points, we performed a B-spline fitting to the center-of-mass coordinates to calculate the actual individual shifts to be performed. Photo-bleaching correction was done by normalization to the average curve obtained upon photo-conversion of Taxol-treated spindles (5 µM, added 20 min before imaging). Background-subtracted and normalized fluorescence of different cells was averaged at each time point and double exponential fitting was performed. The kinetics of fluorescence decay after photo-conversion were analyzed using the equation: $y(t) = A1 \times \exp(-t/t1) + A2 \times \exp(-t/t2) + y0$, where A1 and A2 are the relative populations of kinetochore (more stable) and nonkinetochore (less stable) MT populations with characteristic times of t1 and t2, respectively, and y0 is an offset parameter that accounts for imperfect estimation of background intensity in the normalization step. Half-times are obtained by multiplication by ln(2).

To quantify the abundance of nonkinetochore MTs, z-stacks were acquired of mitotic HeLa cells after different RNAi treatments and immunostaining for the plus-end marker EB1. After maximum intensity projection, the signal within the mitotic spindles was subtracted from the total EB1

signal. MT polymerization rate and stability were measured in HeLa EB1-EGFP cells. Therefore, live-cell imaging was performed on a microscope (TCS-SP5 DMI6000; Leica) with frame-to-frame time intervals of 1 s, and MT plus ends were tracked over time.

For plus-end tracking in HeLa EB3-YFP cells, time series were acquired on a spinning disk microscope (Axio Observer Z1; Carl Zeiss) equipped with CCD camera (Evolve 512; Photometrics), spinning disk dichroic mirror quad band 'RQFT', four laser lines (405, 488, 561, and 639 nm), and motorized emission filter wheel, and using a 100x α-Plan Apochromat NA 1.46 oil immersion objective. Frame-to-frame interval was 400 ms and fluorescence signals were tracked manually using ImageJ (plugin by F.P. Cordelières). To analyze K-fiber stability, medium was exchanged to ice-cold medium and cells were incubated at 4°C for various time intervals ranging from 5 to 20 min. Thereafter, cells were methanol fixed and stained for α-tubulin and kinetochores (CREST antiserum). Integrated pixel intensity of MTs was quantified in MetaMorph 7.0 and normalized to the CREST signal.

Nocodazole sensitivity and monastrol assay

Sensitivity to the spindle poison nocodazole was assessed by transfecting HeLa cells with hKID or KIF4A siRNA for 24 h before the addition of nocodazole (15 nM for 12 h). Thereafter, cells were imaged, counted, and the mitotic index calculated.

For measurement of monopolar spindles, HeLa cells expressing EGFP-centrin1 and α-tubulin–mRFP were transfected with siRNA targeting hKID, KIF4A, or both for 48 h and treated with 100 µM monastrol for 3 h. Methanol-fixed cells were stained for the outer kinetochore marker HEC1 and DNA was visualized using DAPI. Monopolar spindles were imaged as a 3D z-stack using a 100x NA 1.35 oil objective on a DeltaVision microscope (Applied Precision) and deconvolved using softWoRx (Applied Precision). Kinetochores and centrioles were detected using the Imaris spot detection algorithm (Bitplane), and their positions were saved. The distance between kinetochores and the nearest mother centriole was calculated in Excel (Microsoft).

Statistical methods

Descriptive and analytical statistics were performed using R software (www.R-project.org), SPSS 15 for Windows (SPSS Inc.), StatView, or Excel 2007 (Microsoft). Data were evaluated for normal distribution using QQ-plots and the arithmetic mean, median, the standard deviation, and standard error of mean was determined. Student's t tests were performed for data with normal distribution.

Online supplemental material

Fig. S1 shows (A) selected frames from Videos 1–4 of control and chromokinesin knockdown HeLa cells, (B) a quantification of the duration of mitosis in these cells, and (C) a quantification of lagging chromosomes and cytokinesis defects in control and chromokinesin RNAi cells. Fig. S2 shows activation of the mitotic checkpoint in chromokinesin knockdown cells. Fig. S3 shows maximum-intensity projection of confocal z-stacks of control and chromokinesin RNAi cells. Fig. S4 shows the analysis of MT dynamics in EB3-YFP–expressing HeLa cells in control and chromokinesin RNAi experiments, by showing representative mitotic cells (A), MT growth velocity (B), MT life time (C), kinetochore MT cold stability (D), and the radial distance of chromosomes in monopolar spindles in control and chromokinesin knockdown cells (E). Fig. S5 shows the fluorescence decay rates of photo-converted mEos-tubulin in control and chromokinesin knockdown cells (A) and extracted MT half times (B). Videos 1–4 show control histone H2B-GFP–expressing HeLa cells and chromokinesin knockdown cells with images taken every minute. Videos 5–7 show control, hKID, and KIF4A high resolution (images taken every 15 s) movies. Videos 8–10 show high resolution time-lapse recordings of hKID/KIF4A double RNAi cells. Online supplemental material is available at http://www.jcb.org/cgi/content/full/jcb.201110060/DC1.

References

Amaro, A.C., C.P. Samora, R. Holtackers, E. Wang, I.J. Kingston, M. Alonso, M. Lampson, A.D. McAinsh, and P. Meraldi. 2010. Molecular control of kinetochore-microtubule dynamics and chromosome oscillations. *Nat. Cell Biol.* 12:319–329. http://dx.doi.org/10.1038/ncb2033

Antonio, C., I. Ferby, H. Wilhelm, M. Jones, E. Karsenti, A.R. Nebreda, and I. Vernos. 2000. Xkid, a chromokinesin required for chromosome alignment on the metaphase plate. *Cell.* 102:425–435. http://dx.doi.org/10.1016/S0092-8674(00)00048-9

Barisic, M., B. Sohm, P. Mikolcevic, C. Wandke, V. Rauch, T. Ringer, M. Hess, G. Bonn, and S. Geley. 2010. Spindly/CCDC99 is required for efficient chromosome congression and mitotic checkpoint regulation. *Mol. Biol. Cell.* 21:1968–1981. http://dx.doi.org/10.1091/mbc.E09-04-0356

Bieling, P., I. Kronja, and T. Surrey. 2010a. Microtubule motility on reconstituted meiotic chromatin. *Curr. Biol.* 20:763–769. http://dx.doi.org/10.1016/j.cub.2010.02.067

Bieling, P., I.A. Telley, and T. Surrey. 2010b. A minimal midzone protein module controls formation and length of antiparallel microtubule overlaps. *Cell.* 142:420–432. http://dx.doi.org/10.1016/j.cell.2010.06.033

Bringmann, H., G. Skiniotis, A. Spilker, S. Kandels-Lewis, I. Vernos, and T. Surrey. 2004. A kinesin-like motor inhibits microtubule dynamic instability. *Science.* 303:1519–1522. http://dx.doi.org/10.1126/science.1094838

Brouhard, G.J., and A.J. Hunt. 2005. Microtubule movements on the arms of mitotic chromosomes: polar ejection forces quantified in vitro. *Proc. Natl. Acad. Sci. USA.* 102:13903–13908. http://dx.doi.org/10.1073/pnas.0506017102

Buster, D.W., and D.J. Sharp. Chromokinesins Affect the Flux Rate of Mitotic Spindle Microtubules in *Drosophila* S2 Cells. 45th Meeting of the Americal Society of Cell Biology, San Francisco. 2005. Abstract.

Cassimeris, L., C.L. Rieder, and E.D. Salmon. 1994. Microtubule assembly and kinetochore directional instability in vertebrate monopolar spindles: implications for the mechanism of chromosome congression. *J. Cell Sci.* 107:285–297.

Castoldi, M., and I. Vernos. 2006. Chromokinesin Xklp1 contributes to the regulation of microtubule density and organization during spindle assembly. *Mol. Biol. Cell.* 17:1451–1460. http://dx.doi.org/10.1091/mbc.E05-04-0271

Cochran, J.C., C.V. Sindelar, N.K. Mulko, K.A. Collins, S.E. Kong, R.S. Hawley, and F.J. Kull. 2009. ATPase cycle of the nonmotile kinesin NOD allows microtubule end tracking and drives chromosome movement. *Cell.* 136:110–122. http://dx.doi.org/10.1016/j.cell.2008.11.048

Daum, J.R., T.A. Potapova, S. Sivakumar, J.J. Daniel, J.N. Flynn, S. Rankin, and G.J. Gorbsky. 2011. Cohesion fatigue induces chromatid separation in cells delayed at metaphase. *Curr. Biol.* 21:1018–1024. http://dx.doi.org/10.1016/j.cub.2011.05.032

Du, Y., C.A. English, and R. Ohi. 2010. The kinesin-8 Kif18A dampens microtubule plus-end dynamics. *Curr. Biol.* 20:374–380. http://dx.doi.org/10.1016/j.cub.2009.12.049

Funabiki, H., and A.W. Murray. 2000. The Xenopus chromokinesin Xkid is essential for metaphase chromosome alignment and must be degraded to allow anaphase chromosome movement. *Cell.* 102:411–424. http://dx.doi.org/10.1016/S0092-8674(00)00047-7

Ganem, N.J., K. Upton, and D.A. Compton. 2005. Efficient mitosis in human cells lacking poleward microtubule flux. *Curr. Biol.* 15:1827–1832. http://dx.doi.org/10.1016/j.cub.2005.08.065

Gao, J., N. Sai, C. Wang, X. Sheng, Q. Shao, C. Zhou, Y. Shi, S. Sun, X. Qu, and C. Zhu. 2011. Overexpression of chromokinesin KIF4 inhibits proliferation of human gastric carcinoma cells both in vitro and in vivo. *Tumour Biol.* 32:53–61. http://dx.doi.org/10.1007/s13277-010-0090-0

Garcia, M.A., N. Koonrugsa, and T. Toda. 2002. Two kinesin-like Kin I family proteins in fission yeast regulate the establishment of metaphase and the onset of anaphase A. *Curr. Biol.* 12:610–621. http://dx.doi.org/10.1016/S0960-9822(02)00761-3

Gordon, D.J., B. Resio, and D. Pellman. 2012. Causes and consequences of aneuploidy in cancer. *Nat. Rev. Genet.* 13:189–203.

Goshima, G., and R.D. Vale. 2003. The roles of microtubule-based motor proteins in mitosis: comprehensive RNAi analysis in the *Drosophila* S2 cell line. *J. Cell Biol.* 162:1003–1016. http://dx.doi.org/10.1083/jcb.200303022

Gupta, M.L. Jr., P. Carvalho, D.M. Roof, and D. Pellman. 2006. Plus end-specific depolymerase activity of Kip3, a kinesin-8 protein, explains its role in positioning the yeast mitotic spindle. *Nat. Cell Biol.* 8:913–923. http://dx.doi.org/10.1038/ncb1457

Hu, C.K., M. Coughlin, C.M. Field, and T.J. Mitchison. 2011. KIF4 regulates midzone length during cytokinesis. *Curr. Biol.* 21:815–824. http://dx.doi.org/10.1016/j.cub.2011.04.019

Hu, C.K., M. Coughlin, and T.J. Mitchison. 2012. Midbody assembly and its regulation during cytokinesis. *Mol. Biol. Cell.* 23:1024–1034. http://dx.doi.org/10.1091/mbc.E11-08-0721

Jaqaman, K., E.M. King, A.C. Amaro, J.R. Winter, J.F. Dorn, H.L. Elliott, N. McHedlishvili, S.E. McClelland, I.M. Porter, M. Posch, et al. 2010. Kinetochore alignment within the metaphase plate is regulated by centromere stiffness and microtubule depolymerases. *J. Cell Biol.* 188:665–679. http://dx.doi.org/10.1083/jcb.200909005

Jordan, M.A., D. Thrower, and L. Wilson. 1992. Effects of vinblastine, podophyllotoxin and nocodazole on mitotic spindles. Implications for the role of microtubule dynamics in mitosis. *J. Cell Sci.* 102:401–416.

Kapoor, T.M., and D.A. Compton. 2002. Searching for the middle ground: mechanisms of chromosome alignment during mitosis. *J. Cell Biol.* 157:551–556. http://dx.doi.org/10.1083/jcb.200202073

Kapoor, T.M., M.A. Lampson, P. Hergert, L. Cameron, D. Cimini, E.D. Salmon, B.F. McEwen, and A. Khodjakov. 2006. Chromosomes can congress to the metaphase plate before biorientation. *Science.* 311:388–391. http://dx.doi.org/10.1126/science.1122142

Ke, K., J. Cheng, and A.J. Hunt. 2009. The distribution of polar ejection forces determines the amplitude of chromosome directional instability. *Curr. Biol.* 19:807–815. http://dx.doi.org/10.1016/j.cub.2009.04.036

Kim, Y., A.J. Holland, W. Lan, and D.W. Cleveland. 2010. Aurora kinases and protein phosphatase 1 mediate chromosome congression through regulation of CENP-E. *Cell.* 142:444–455. http://dx.doi.org/10.1016/j.cell.2010.06.039

Kurasawa, Y., W.C. Earnshaw, Y. Mochizuki, N. Dohmae, and K. Todokoro. 2004. Essential roles of KIF4 and its binding partner PRC1 in organized central spindle midzone formation. *EMBO J.* 23:3237–3248. http://dx.doi.org/10.1038/sj.emboj.7600347

Kwon, M., S. Morales-Mulia, I. Brust-Mascher, G.C. Rogers, D.J. Sharp, and J.M. Scholey. 2004. The chromokinesin, KLP3A, dives mitotic spindle pole separation during prometaphase and anaphase and facilitates chromatid motility. *Mol. Biol. Cell.* 15:219–233. http://dx.doi.org/10.1091/mbc.E03-07-0489

Levesque, A.A., and D.A. Compton. 2001. The chromokinesin Kid is necessary for chromosome arm orientation and oscillation, but not congression, on mitotic spindles. *J. Cell Biol.* 154:1135–1146. http://dx.doi.org/10.1083/jcb.200106093

Levesque, A.A., L. Howard, M.B. Gordon, and D.A. Compton. 2003. A functional relationship between NuMA and kid is involved in both spindle organization and chromosome alignment in vertebrate cells. *Mol. Biol. Cell.* 14:3541–3552. http://dx.doi.org/10.1091/mbc.E03-02-0082

Logarinho, E., S. Maffini, M. Barisic, A. Marques, A. Toso, P. Meraldi, and H. Maiato. 2012. CLASPs prevent irreversible multipolarity by ensuring spindle-pole resistance to traction forces during chromosome alignment. *Nat. Cell Biol.* 14:295–303. http://dx.doi.org/10.1038/ncb2423

Magidson, V., C.B. O'Connell, J. Lončarek, R. Paul, A. Mogilner, and A. Khodjakov. 2011. The spatial arrangement of chromosomes during prometaphase facilitates spindle assembly. *Cell.* 146:555–567. http://dx.doi.org/10.1016/j.cell.2011.07.012

Marshall, W.F., J.F. Marko, D.A. Agard, and J.W. Sedat. 2001. Chromosome elasticity and mitotic polar ejection force measured in living *Drosophila* embryos by four-dimensional microscopy-based motion analysis. *Curr. Biol.* 11:569–578. http://dx.doi.org/10.1016/S0960-9822(01)00180-4

Martin-Lluesma, S., V.M. Stucke, and E.A. Nigg. 2002. Role of Hec1 in spindle checkpoint signaling and kinetochore recruitment of Mad1/Mad2. *Science.* 297:2267–2270. http://dx.doi.org/10.1126/science.1075596

Matos, I., A.J. Pereira, M. Lince-Faria, L.A. Cameron, E.D. Salmon, and H. Maiato. 2009. Synchronizing chromosome segregation by flux-dependent force equalization at kinetochores. *J. Cell Biol.* 186:11–26. http://dx.doi.org/10.1083/jcb.200904153

Mayr, M.I., S. Hümmer, J. Bormann, T. Grüner, S. Adio, G. Woehlke, and T.U. Mayer. 2007. The human kinesin Kif18A is a motile microtubule depolymerase essential for chromosome congression. *Curr. Biol.* 17:488–498. http://dx.doi.org/10.1016/j.cub.2007.02.036

Mazumdar, M., and T. Misteli. 2005. Chromokinesins: multitalented players in mitosis. *Trends Cell Biol.* 15:349–355. http://dx.doi.org/10.1016/j.tcb.2005.05.006

Mazumdar, M., S. Sundareshan, and T. Misteli. 2004. Human chromokinesin KIF4A functions in chromosome condensation and segregation. *J. Cell Biol.* 166:613–620. http://dx.doi.org/10.1083/jcb.200401142

Mazumdar, M., J.H. Lee, K. Sengupta, T. Ried, S. Rane, and T. Misteli. 2006. Tumor formation via loss of a molecular motor protein. *Curr. Biol.* 16:1559–1564. http://dx.doi.org/10.1016/j.cub.2006.06.029

McKinney, S.A., C.S. Murphy, K.L. Hazelwood, M.W. Davidson, and L.L. Looger. 2009. A bright and photostable photoconvertible fluorescent protein. *Nat. Methods.* 6:131–133. http://dx.doi.org/10.1038/nmeth.1296

Midorikawa, R., Y. Takei, and N. Hirokawa. 2006. KIF4 motor regulates activity-dependent neuronal survival by suppressing PARP-1 enzymatic activity. *Cell.* 125:371–383. http://dx.doi.org/10.1016/j.cell.2006.02.039

Nasmyth, K. 2002. Segregating sister genomes: the molecular biology of chromosome separation. *Science.* 297:559–565. http://dx.doi.org/10.1126/science.1074757

Ohsugi, M., K. Adachi, R. Horai, S. Kakuta, K. Sudo, H. Kotaki, N. Tokai-Nishizumi, H. Sagara, Y. Iwakura, and T. Yamamoto. 2008. Kid-mediated chromosome compaction ensures proper nuclear envelope formation. *Cell.* 132:771–782. http://dx.doi.org/10.1016/j.cell.2008.01.029

Oshimori, N., M. Ohsugi, and T. Yamamoto. 2006. The Plk1 target Kizuna stabilizes mitotic centrosomes to ensure spindle bipolarity. *Nat. Cell Biol.* 8:1095–1101. http://dx.doi.org/10.1038/ncb1474

Powers, J., D.J. Rose, A. Saunders, S. Dunkelbarger, S. Strome, and W.M. Saxton. 2004. Loss of KLP-19 polar ejection force causes misorientation and missegregation of holocentric chromosomes. *J. Cell Biol.* 166:991–1001. http://dx.doi.org/10.1083/jcb.200403036

Ribeiro, S.A., J.C. Gatlin, Y. Dong, A. Joglekar, L. Cameron, D.F. Hudson, C.J. Farr, B.F. McEwen, E.D. Salmon, W.C. Earnshaw, and P. Vagnarelli. 2009. Condensin regulates the stiffness of vertebrate centromeres. *Mol. Biol. Cell.* 20:2371–2380. http://dx.doi.org/10.1091/mbc.E08-11-1127

Rieder, C.L., and G.G. Borisy. 1981. The attachment of kinetochores to the prometaphase spindle in PtK1 cells. Recovery from low temperature treatment. *Chromosoma.* 82:693–716. http://dx.doi.org/10.1007/BF00285776

Rieder, C.L., and E.D. Salmon. 1994. Motile kinetochores and polar ejection forces dictate chromosome position on the vertebrate mitotic spindle. *J. Cell Biol.* 124:223–233. http://dx.doi.org/10.1083/jcb.124.3.223

Rieder, C.L., E.A. Davison, L.C. Jensen, L. Cassimeris, and E.D. Salmon. 1986. Oscillatory movements of monooriented chromosomes and their position relative to the spindle pole result from the ejection properties of the aster and half-spindle. *J. Cell Biol.* 103:581–591. http://dx.doi.org/10.1083/jcb.103.2.581

Santamaria, A., S. Nagel, H.H. Sillje, and E.A. Nigg. 2008. The spindle protein CHICA mediates localization of the chromokinesin Kid to the mitotic spindle. *Curr. Biol.* 18:723–729. http://dx.doi.org/10.1016/j.cub.2008.04.041

Stevens, D., R. Gassmann, K. Oegema, and A. Desai. 2011. Uncoordinated loss of chromatid cohesion is a common outcome of extended metaphase arrest. *PLoS ONE.* 6:e22969. http://dx.doi.org/10.1371/journal.pone.0022969

Stumpff, J., G. von Dassow, M. Wagenbach, C. Asbury, and L. Wordeman. 2008. The kinesin-8 motor Kif18A suppresses kinetochore movements to control mitotic chromosome alignment. *Dev. Cell.* 14:252–262. http://dx.doi.org/10.1016/j.devcel.2007.11.014

Stumpff, J., Y. Du, C.A. English, Z. Maliga, M. Wagenbach, C.L. Asbury, L. Wordeman, and R. Ohi. 2011. A tethering mechanism controls the processivity and kinetochore-microtubule plus-end enrichment of the kinesin-8 Kif18A. *Mol. Cell.* 43:764–775. http://dx.doi.org/10.1016/j.molcel.2011.07.022

Stumpff, J., M. Wagenbach, A. Franck, C.L. Asbury, and L. Wordeman. 2012. Kif18A and chromokinesins confine centromere movements via microtubule growth suppression and spatial control of kinetochore tension. *Dev. Cell.* 22:1017–1029. http://dx.doi.org/10.1016/j.devcel.2012.02.013

Theurkauf, W.E., and R.S. Hawley. 1992. Meiotic spindle assembly in *Drosophila* females: behavior of nonexchange chromosomes and the effects of mutations in the nod kinesin-like protein. *J. Cell Biol.* 116:1167–1180. http://dx.doi.org/10.1083/jcb.116.5.1167

Tokai-Nishizumi, N., M. Ohsugi, E. Suzuki, and T. Yamamoto. 2005. The chromokinesin Kid is required for maintenance of proper metaphase spindle size. *Mol. Biol. Cell.* 16:5455–5463. http://dx.doi.org/10.1091/mbc.E05-03-0244

Varga, V., J. Helenius, K. Tanaka, A.A. Hyman, T.U. Tanaka, and J. Howard. 2006. Yeast kinesin-8 depolymerizes microtubules in a length-dependent manner. *Nat. Cell Biol.* 8:957–962. http://dx.doi.org/10.1038/ncb1462

Vernos, I., J. Raats, T. Hirano, J. Heasman, E. Karsenti, and C. Wylie. 1995. Xklp1, a chromosomal Xenopus kinesin-like protein essential for spindle organization and chromosome positioning. *Cell.* 81:117–127. http://dx.doi.org/10.1016/0092-8674(95)90376-3

Wan, X., D. Cimini, L.A. Cameron, and E.D. Salmon. 2012. The coupling between sister kinetochore directional instability and oscillations in centromere stretch in metaphase PtK1 cells. *Mol. Biol. Cell.* 23:1035–1046. http://dx.doi.org/10.1091/mbc.E11-09-0767

Wandke, C., and S. Geley. 2006. Generation and characterization of an hKid-specific monoclonal antibody. *Hybridoma (Larchmt).* 25:41–43. http://dx.doi.org/10.1089/hyb.2006.25.41

Wargacki, M.M., J.C. Tay, E.G. Muller, C.L. Asbury, and T.N. Davis. 2010. Kip3, the yeast kinesin-8, is required for clustering of kinetochores at metaphase. *Cell Cycle.* 9:2581–2588. http://dx.doi.org/10.4161/cc.9.13.12076

West, R.R., T. Malmstrom, and J.R. McIntosh. 2002. Kinesins klp5(+) and klp6(+) are required for normal chromosome movement in mitosis. *J. Cell Sci.* 115:931–940.

Williams, B.C., M.F. Riedy, E.V. Williams, M. Gatti, and M.L. Goldberg. 1995. The *Drosophila* kinesin-like protein KLP3A is a midbody component required for central spindle assembly and initiation of cytokinesis. *J. Cell Biol.* 129:709–723. http://dx.doi.org/10.1083/jcb.129.3.709

Wolf, F., C. Wandke, N. Isenberg, and S. Geley. 2006. Dose-dependent effects of stable cyclin B1 on progression through mitosis in human cells. *EMBO J.* 25:2802–2813. http://dx.doi.org/10.1038/sj.emboj.7601163

Yajima, J., M. Edamatsu, J. Watai-Nishii, N. Tokai-Nishizumi, T. Yamamoto, and Y.Y. Toyoshima. 2003. The human chromokinesin Kid is a plus end-directed microtubule-based motor. *EMBO J.* 22:1067–1074. http://dx.doi.org/10.1093/emboj/cdg102

Zhu, C., and W. Jiang. 2005. Cell cycle-dependent translocation of PRC1 on the spindle by Kif4 is essential for midzone formation and cytokinesis. *Proc. Natl. Acad. Sci. USA.* 102:343–348. http://dx.doi.org/10.1073/pnas.0408438102

Zhu, C., J. Zhao, M. Bibikova, J.D. Leverson, E. Bossy-Wetzel, J.B. Fan, R.T. Abraham, and W. Jiang. 2005. Functional analysis of human microtubule-based motor proteins, the kinesins and dyneins, in mitosis/cytokinesis using RNA interference. *Mol. Biol. Cell.* 16:3187–3199. http://dx.doi.org/10.1091/mbc.E05-02-0167